RESEARCH LABORATORIES FOR THE ENGINEERING SCIENCES

SCHOOL OF ENGINEERING AND APPLIED SCIENCE

University of Virginia

Charlottesville, Virginia 22901

POST-FAILURE PHENOMENA IN LMFBR TOP ACCIDENTS

Annual Report
July 1, 1975 - June 30, 1976

by

C. A. Erdman, M. B. Johnson, and A. B. Reynolds

Prepared for the U. S. Nuclear Regulatory Commission
Washington, D. C. 20555
Under Contract No. AT(49-24)-0158

Report No. UVA/529058/NE77/101
Revised January 1977

RESEARCH LABORATORIES FOR THE ENGINEERING SCIENCES

Members of the faculty who teach at the undergraduate and graduate levels and a number of professional engineers and scientists whose primary activity is research generate and conduct the investigations that make up the school's research program. The School of Engineering and Applied Science of the University of Virginia believes that research goes hand in hand with teaching. Early in the development of its graduate training program, the School recognized that men and women engaged in research should be as free as possible of the administrative duties involved in sponsored research. In 1959, therefore, the Research Laboratories for the Engineering Sciences (RLES) was established and assigned the administrative responsibility for such research within the School.

The director of RLES—himself a faculty member and researcher—maintains familiarity with the support requirements of the research under way. He is aided by an Academic Advisory Committee made up of a faculty representative from each academic department of the School. This Committee serves to inform RLES of the needs and perspectives of the research program.

In addition to administrative support, RLES is charged with providing certain technical assistance. Because it is not practical for each department to become self-sufficient in all phases of the supporting technology essential to present-day research, RLES makes services available through the following support groups: Machine Shop, Instrumentation, Facilities Services, Publications (including photographic facilities), and Computer Terminal Maintenance.

POST-FAILURE PHENOMENA IN LMFBR TOP ACCIDENTS

Annual Report
July 1, 1975 - June 30, 1976

by

C. A. Erdman, M. B. Johnson, and A. B. Reynolds

Prepared for the U. S. Nuclear Regulatory Commission
Washington, D. C. 20555
Under Contract No. AT(49-24)-0158

Department of Nuclear Engineering
RESEARCH LABORATORIES FOR THE ENGINEERING SCIENCES
SCHOOL OF ENGINEERING AND APPLIED SCIENCE
UNIVERSITY OF VIRGINIA
CHARLOTTESVILLE, VIRGINIA

Report No. UVA/529058/NE77/101
Revised January 1977

Copy No. 5

TABLE OF CONTENTS

TABLE OF CONTENTS (cont.)

ABSTRACT

The work reported here was primarily aimed at establishing minimum requirements for and likelihood of large-scale voiding following fuel-pin-failure in an unprotected transient overpower (TOP) accident in a liquid-metal-cooled fast breeder reactor (LMFBR). Some attention was also given to voiding following pin failure in the low power channels of an LMFBR during the loss-of-flow-driven TOP. Initial work on early fuel motion out the pin and into sodium for both types of TOP accidents is also discussed.

I. SUMMARY

The work plan for the fiscal year (FY76) was completed essentially as originally proposed. Emphasis was, however, shifted somewhat among activities as a result of discussions with DPM personnel during the year.

The primary goal for the year was a determination of the minimum requirements for and likelihood of large-scale subassembly voiding following pin failure in the transient overpower (TOP) accident. The motivation was to investigate the possibility of late-ejected fuel entering a voided region and therefore not being easily fragmented and swept out of the coolant channels. The approach taken was two-fold: (1) look at important physical phenomena (e.g. prefailure fuel motion, fuel fragmentation, etc.) in an isolated manner when possible, and (2) use the results of these phenomena studies to select input for a parametric code which models fuel-coolant-interactions (FCI) in subassembly geometries. However, some of the work associated with the parametric approach was performed relatively early in the contract year to provide additional guidance in selection of the important physical phenomena. (These early calculations are discussed in less detail than the later work.)

The major conclusions drawn from the work for FY76 are as follows:

- Ejected molten fuel masses in the range of 5 to 10 g/pin are sufficient to produce large-scale voiding under good fragmentation and mixing conditions for the classical transient overpower (TOP) accident.
- Either hydrodynamic or thermal fragmentation appears to be capable of producing the necessary fragmentation and mixing condtions in the TOP accident.
- For situations in which large amounts of molten fuel (e.g. ~ 10 g/pin) are released into coolant channel sodium, the most important factor governing voiding dynamics, is, as anticipated, fuel particle size.
- For situations in which small amounts of fuel (e.g. < 5 g/pin) are involved, the key parameter for maintaining extended voiding is initial cladding temperature.
- For the loss-of-flow-driven-TOP (LOF-D-TOP), at least three potential mechanisms could give extensive, long-term voiding: FCI, sodium squeeze-out, and plenum gas release.

• Plenum-gas-induced voiding on initial failure in the classical TOP appears milder than expected, especially in terms of plenum pressures anticipated for the first CRBR core.

• The effects of two-dimensional (2D) voiding within a subassembly resulting from failure of only the central pins are manifested primarily in terms of available flow areas and condensing surfaces.

In addition to the specific technical work indicated above, other consulting services were provided at DPM's request. These included meeting attendance (with trip reports) at DPM's request, suggested responses to interrogatories, and on-call consultation and discussion.

2. IMPORTANT FACTORS IN VOIDING DUE TO FCI IN THE CLASSICAL TOP

In order to produce extensive voiding in an FCI, significant energy must be present in the molten fuel ejected from the pins and must be transferred to the coolant on a reasonable time scale. The energy in ejected molten fuel is a function of both mass and temperature; increasing the energy (referenced to solidus) of a quantity of fuel at a temperature of 3500 K by 10% requires either a mass increase of 10% or a temperature increase of 100 K. Doubling the energy of that fuel would require twice the mass or a temperature increase of over 1000 K. In analyzing FCI's, the uncertainty in molten fuel temperatures will be much less than 1000 K; however, the masses of fuel involved will be uncertain by factors greater than two. Thus the key quantity to look at in characterizing energy in molten fuel is the mass of fuel involved.

The time scale for heat transfer from fuel to coolant will be controlled by the characteristic fuel dimensions in regions where the coolant void fraction is small. Large particle dimensions will reduce heat transfer rates and can prohibit voiding. Small dimensions produce vigorous voiding, assuming sufficient fuel is available. Introduction of the same amount of fuel over very long mixing times (e.g. 0.1 s), even in the form of very small particles, will reduce the strength of the voiding under reasonable assumptions for heat transfer in a partially voided region.

The overall voiding dynamics are determined by a tradeoff between heat transfer from fuel to sodium and heat transfer from sodium to cladding. A few simple arguments will demonstrate the factors involved in producing and maintaining extensive voiding for a long period of time.

2.1 Comparison of Heat Fluxes

Consider a mass of fuel, M_f, consisting of particles of radius R. The number of particles, N_f, is then given by

$$N_f = \frac{M_f}{\rho_f \frac{4}{3}\pi R^3}$$

where ρ_f is the fuel density. The total area associated with the

particles is

$$4\pi R^2 N_f = \frac{M_f 4\pi R^2}{\rho_f \frac{4}{3}\pi R^3} = \frac{3M_f}{\rho_f R} .$$

The heat transfer rate, Q_1, from fuel to sodium is given by

$$Q_1 = \left(T_f - T_{Na}\right)\left(\frac{3M_f}{\rho_f R}\right)\left(\frac{k_f}{FR}\right)\left(1 - \alpha\right)$$

for the case of fuel-conduction-limited heat transfer, where F is a number between 0 and 1. The most appropriate value for F can be argued to lie between 0.2 and 0.5. Other terms are as defined below:

T_f = temperature of fuel
T_{Na} = temperature of sodium
k_f = thermal conductivity of fuel
α = void fraction in FCI zone.

Consider the fuel to initially be mixed with liquid sodium in a length L of the coolant channel. The length of the FCI zone at later times is approximately given by $L/(1 - \alpha)$. Thus the heat transfer rate, Q_2, from sodium to cladding is given by

$$Q_2 = (T_{Na} - T_c)\frac{hLP}{(1 - \alpha)}$$

where T_c = temperature of cladding
h = sodium-to-cladding heat transfer coefficient
P = wetted perimeter.

Note that Q_1/Q_2 is proportional to $(1 - \alpha)^2$. Thus as voiding proceeds, the heat addition and loss rates for the sodium become more and more biased toward net loss to the cladding. For example*, for F = .2, k_f/ρ_f = .0029 W·cm²/g·K, L = 10 cm, R = 100 μm = 10^{-2} cm, h = 5.674 W/K·cm², P = 2.46 cm, and M_f is in grams, we find

$$\frac{Q_1}{Q_2} = 3.117\ M_f \left(\frac{T_f - T_{Na}}{T_{Na} - T_c}\right)(1 - \alpha)^2.$$

*The choice of values for F and R is discussed in Appendix B.

Thus, for equal temperature differences and 1.0 g of fuel, an α of only 0.434 would be sufficient for the heat fluxes to balance. For 10.0 g of fuel, the corresponding α for $Q_1/Q_2 = 1.0$ would be 0.821, so the mass of fuel involved is crucial. For the initial zone length of 10 cm considered above, the FCI zones would extend over about 18 cm and 56 cm for the cases of 1.0 and 10.0 g masses of fuel respectively when $Q_1/Q_2 = 1.0$.

2.2 Magnitude of Cladding Heat Capacity

The above calculations illustrate the role that cladding can play as a heat sink for situations involving extensive voiding. This role is further enhanced by the large heat capacity of the available cladding.

The mass of cladding per centimeter length of a single FFTF-type fuel pin is 0.53 g. The heat capacity of that one centimeter length is about 0.27 J/K. Thus the heat capacity per pin available in the active core of CRBR is about 25 J/K. This should be balanced against (ignoring the role of sodium again for the moment) a heat capacity of the order of 0.548 J/g•K for molten fuel. The magnitude of this cladding heat sink can be simply illustrated by considering 10 g of molten fuel at 3500 K. If all of the energy required to cool this fuel to the solidus were uniformly added to the active core cladding of a single pin, the net temperature rise would be 225 K. If the cladding was initially at 1000 K and was allowed to reach thermal equilibrium with the fuel, the final temperature would be about 1500 K.

2.3 Energy in FCI Zone Sodium

In Sections 2.1 and 2.2 above, we ignored the role of sodium as an energy sink in extensive voiding. This can be argued from consideration of the enthalpy of vaporization of enough sodium to completely void the active core. Considering a sodium pressure of 20 atmospheres, only 0.08 g of saturated sodium vapor per pin would completely fill the coolant channels in the active core region. The energy required to convert .08 g of sodium at 1000 K to saturated vapor at 20 atmospheres is about 330 J, which is roughly the heat of fusion of one gram of fuel. Therefore, if we are talking about several grams of fuel which is

initially several hundred degrees above the liquidus, the energy involved in the necessary sodium vaporization would be small compared to the total energy content of the fuel.

It is possible to artificially mitigate the effects of even several grams of fuel per pin by arbitrarily mixing large masses of liquid sodium with the fuel. However, the amounts of sodium which would be involved in a vigorous FCI (i.e. early flow reversal) are fairly small, perhaps 1 to 2 g. The sensible heat involved in raising one gram of saturated liquid sodium at 1000 K to saturated vapor at 1625 K (vapor pressure ~ 25 atm.) is only 840 J. This is less than the energy loss (~ 1090 J) required to convert one gram of molten fuel at 3500 K to solid fuel at 2000 K.

Concerning the masses of sodium which are involved per pin, note that 1 g of liquid sodium at 1000 K would fill 6.5 cm of channel length. Thus the 1.6 g considered in most cases presented in Section 3 of this report represents a channel length of about 10 cm. Having more than this mass of sodium involved in a vigorous FCI which produces early flow reversal seems unlikely. If sodium masses of the order of 1.6 g are considered, then for cases which involve several grams of fuel initially at a temperature several hundreds of degrees above the liquidus, both the sensible heat and energy of vaporization involved in FCI zone sodium will be relatively unimportant compared to cladding heat sink effects.

2.4 Required Pressure History for Extensive Downward Voiding

The normal sodium flow in a CRBR subassembly can be stopped with a relatively small net downward impulse, e.g. the order of 0.1 atm·s. This corresponds to an overpressure of 10 atm for 0.01 s or some similar combination.

For the classical TOP, the sodium driving force from the primary pumps is available to oppose downward voiding. The resulting pressure at the subassembly inlet will be the order of 7.6 atm in CRBR. Therefore FCI zone pressures of the order of 8 atm must be maintained for a reasonable time even after flow reversal has occurred in order to void downward.

From the above discussion it is clear that FCI zone pressures need not be enormous in order to initiate and maintain extensive voiding. For example, an average FCI zone pressure of 20 atm during the first dozen milliseconds would produce flow reversal and initiate downward voiding, after which a pressure of the order of 10 atm would maintain the voiding.

The sodium temperature required to produce a vapor pressure of 10 atm is about 1475 K. The saturation temperature at 20 atm is about 1625 K. (The melting point of cladding is 1645 K.) It will be easier to maintain these temperatures via heat transfer from fuel to sodium while the FCI zone is short in length (see Section 2.1), and heat transfer from the sodium to the cladding is relatively small. However, if the cladding temperatures were to reach the 1400 K to 1500 K range, the cladding could actually pump up the sodium to maintain voiding.

2.5 Summary of Factors Governing FCI Voiding

From the discussions presented above in this section, several statements can be made concerning the possibility of extensive subassembly voiding due to an FCI.

(1) The energy needed to vaporize sufficient amounts of sodium to void the active core is small and corresponds to the heat of fusion of approximately one gram of fuel per pin.

(2) Fuel-to-sodium heat transfer rates must be sufficiently high to produce and maintain sodium temperatures in the neighborhood of 1500 K. These rates are proportional to the mass of fuel interacting and inversely proportional to the square of the characteristic fuel particle dimension.

(3) The sodium-to-cladding heat losses will become important at large FCI zone void fractions even for small fuel particle sizes; however, if the cladding temperature becomes too high, the cladding may actually be holding up the sodium temperature in some parts of the FCI zone.

The statements made above have been verified during the contract year by several series of calculations utilizing a modified version of

the UVAFCI code. The code modifications and the calculational results are presented in Section 3.

3. PARAMETRIC CALCULATIONS - DEFINITION PHASE

In order to investigate the relative importance of various factors in the voiding due to an FCI, the UVAFCI code was modified for use in parametric calculations of subassembly voiding. The modifications are discussed briefly below, followed by a presentation and discussion of the calculational results.

3.1 UVAFCI Modifications

As mentioned in our second and third quarterly reports[1,2] two major modifications were made to the UVAFCI code to model subassembly voiding. First, improved constraint equations were added to permit simulation of CRBR-type flow geometries. Multiple area changes within the flow channels were modeled as suggested in Reference 3, including the effects of orificing. The other major modification was the adaptation of the condensation heat transfer module developed by P. M. Haas[4] to subassembly geometry. The module was rewritten to accommodate downward as well as upward voiding and to account for reentry of sodium from either direction. In a separate effort to ease man-hour requirements for analyzing cases, a plotting routine developed by P. L. Garner was utilized in the latter part of the contract period.

The validity of the calculational results from the modified code have been checked by comparison with simple hand calculations. Some of the results presented below were generated without utilizing the complete capabilities of the modified code, e.g. the studies of Section 3.2 were made without condensation or multiple area changes.

3.2 Voiding Without Condensation on Cladding

The results presented here support the contention of Section 2.3 that little energy is required to heat up and vaporize sufficient sodium to void the active core. Figure 3.1 is a reproduction of Figure 2 from our second quarterly[1]. (One statement made in that report should be corrected. The diameter of the fragmented fuel for the cases presented was 252 microns rather than 200 microns. Also, the value used for the

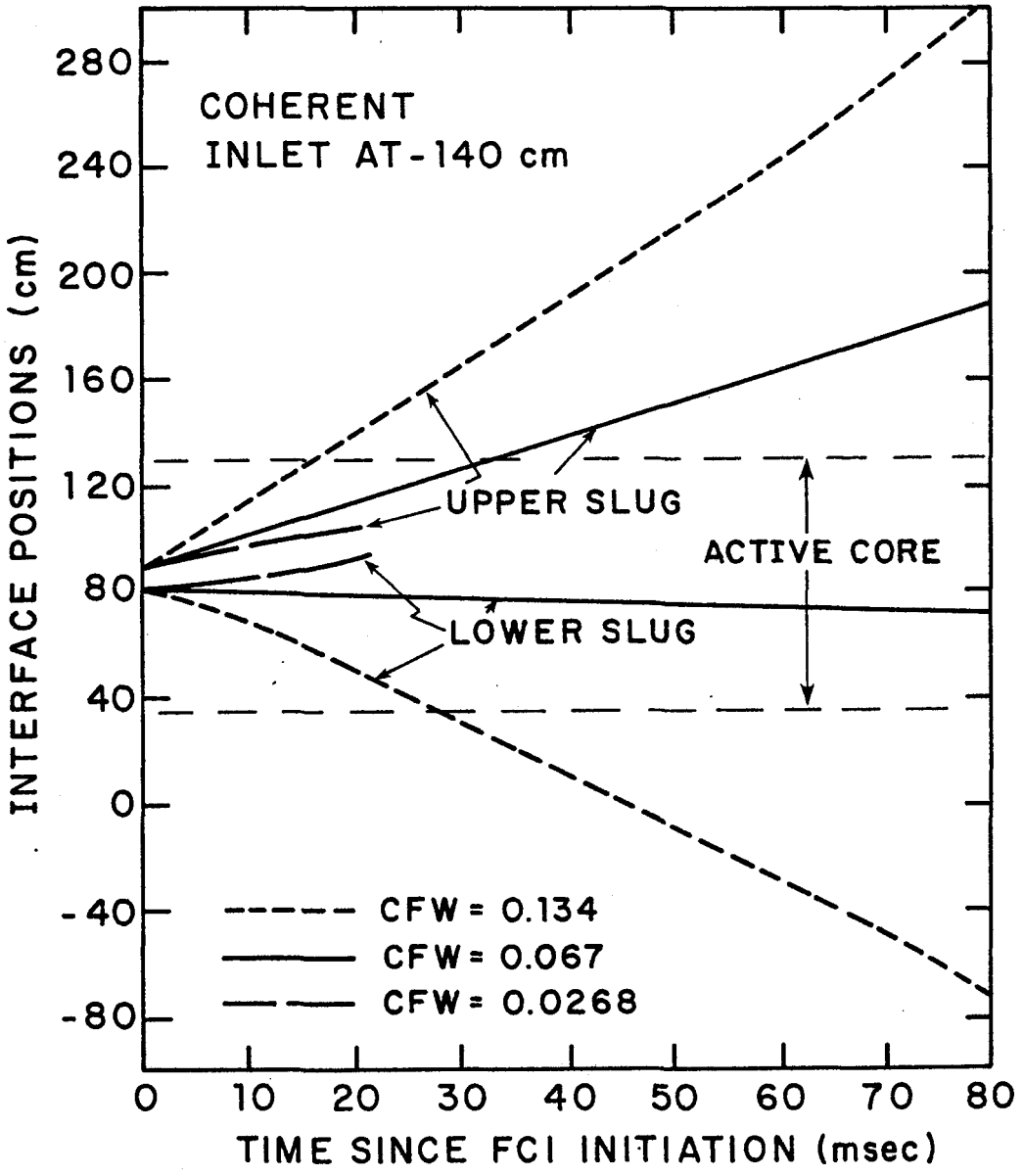

Figure 3.1 Effect of mass of fuel initially ejected on subsequent voiding histories (no zone-to-cladding heat losses).

parameter CFW corresponds to a fuel to sodium ratio of 1.02 rather than unity. These corrections resulted from a reevaluation of fuel properties.) The case for which CFW = .134 corresponds to the interaction of approximately 1.6 g of fuel initially at 3500 K with 1.6 g of sodium initially at 940 K. Note from the figure that as the fuel mass is reduced to 0.8 g (CFW = 0.67) downward voiding is negligible, and for 0.33 g of fuel (CFW = .0268), the interaction is extremely mild.

3.3 Consideration of Sodium Condensation on Zone Cladding

Condensation heat losses to FCI zone cladding can dramatically change the voiding histories. This is illustrated in Figure 3.2. The curve labeled "no heat losses to cladding" in Figure 3.2 is very similar to the case with CFW = .134 in Figure 3.1. (The major difference is the location of the channel inlet relative to the bottom of the lower blanket. This is -140 cm for Figure 3.1 and -95 cm for Figure 3.2.) When condensation is accounted for, the reduction in voiding is dramatic. The initial FCI zone location (extending from 80 cm to 90 cm, referenced to the bottom of the lower blanket) is covered by the lower sodium slug at about 55 milliseconds. The condensation heat transfer coefficient was taken as 5.674 $W/cm^2 \cdot K$; the choice of this coefficient is discussed in Appendix B.

Results such as those of Figure 3.2 indicated that much larger masses of fuel per pin must be involved in the FCI than the 1.6 g of fuel used in generating the Figure 3.2 results. Therefore, a value of 3.2 g/pin was selected for use in a series of calculations which looked at the effects of various other parameters on voiding dynamics.

3.4 Second Order Effects in FCI Voiding

A reference case, designated 1B for purposes of this report, was selected in order to look at the effects of various parameters on the predicted FCI voiding. The important parameters* for the 1B run are given below:

Interacting masses

fuel = 3.2 g

sodium = 1.6 g

*The tables of Appendix C summarize parameter values for the runs discussed in Sections 3.4 and 3.5.

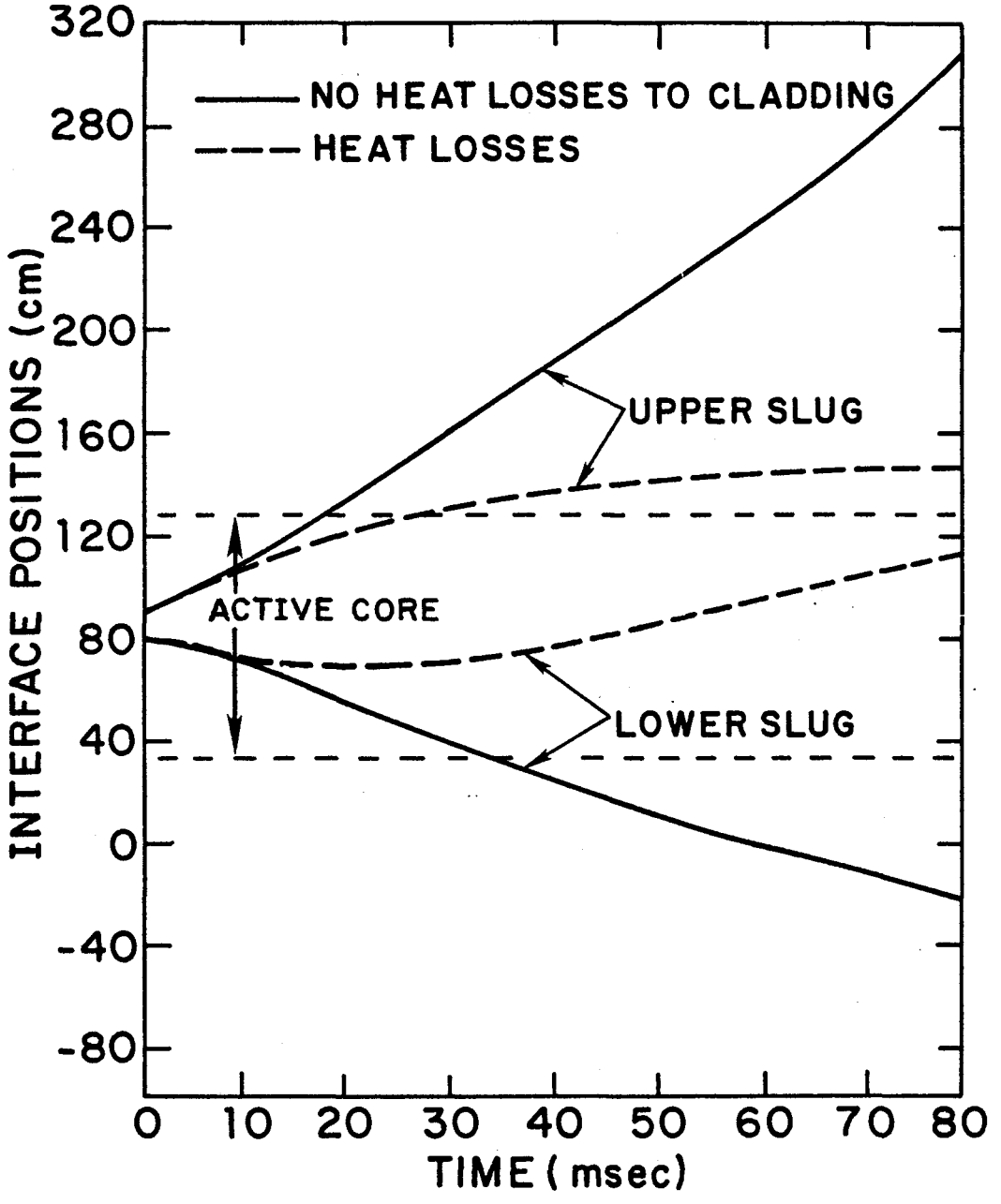

Figure 3.2 Effect of zone-to-cladding heat transfer on voiding histories.

Initial temperatures

fuel = 3500 K

sodium = 940 K

Fuel particle diameter = 250 μm

Sodium-to-cladding heat transfer coefficient = 5.674 $W/cm^2 \cdot K$

Mixing time = 0.0 s (coherent)

The effect of variations in sodium masses from the base case is shown in Figure 3.3. The case labeled 3G had half as much sodium, i.e. 0.8 g, as 1B. Note that the reduction in sodium mass has only a slight effect on the voiding history. The effect of doubling the sodium mass to 3.2 g is shown by case 3B. Once again the effect on voiding history is slight. It is clear that the mass of sodium involved is a second order effect as suggested in Section 2.3.

Case 1B and most of the other cases run during the year assumed an initial FCI zone location beginning at 80 cm and extending to 90 cm above the bottom of the lower blanket. Shifting this location upward by 50 cm (which placed the initial FCI zone partially in the upper blanket) served only to shift the voiding patterns upward by 50 cm. This is illustrated by Figure 3.4, where 1B results are plotted against a case (8F) for which the initial FCI zone boundaries are 130 and 140 cm.

The presence of non-condensable gasses in the FCI zone can mitigate the voiding if the gas is assumed to initially be at a low pressure. This is illustrated by Figure 3.5, in which case 1B (with no cushion gas) is compared with case 4E, in which 0.8 cc of gas at 10 atm pressure is initially present in the zone. Even for such low initial pressures, the effect on voiding history is small. As the initial gas pressure is increased, the benefits of the cushion gas disappear.

In work performed this past year, the effects of varying fuel-sodium mixing times were small over the range of mixing times of interest. We were only interested in the first few grams of fuel (certainly less than 10 g) which leave the pin. Both PLUTO and SAS calculations[5] indicated that the order of 1 gram of fuel per pin per millisecond was a reasonable ejection rate during the first few milliseconds. Thus for the conditions of interest to us,

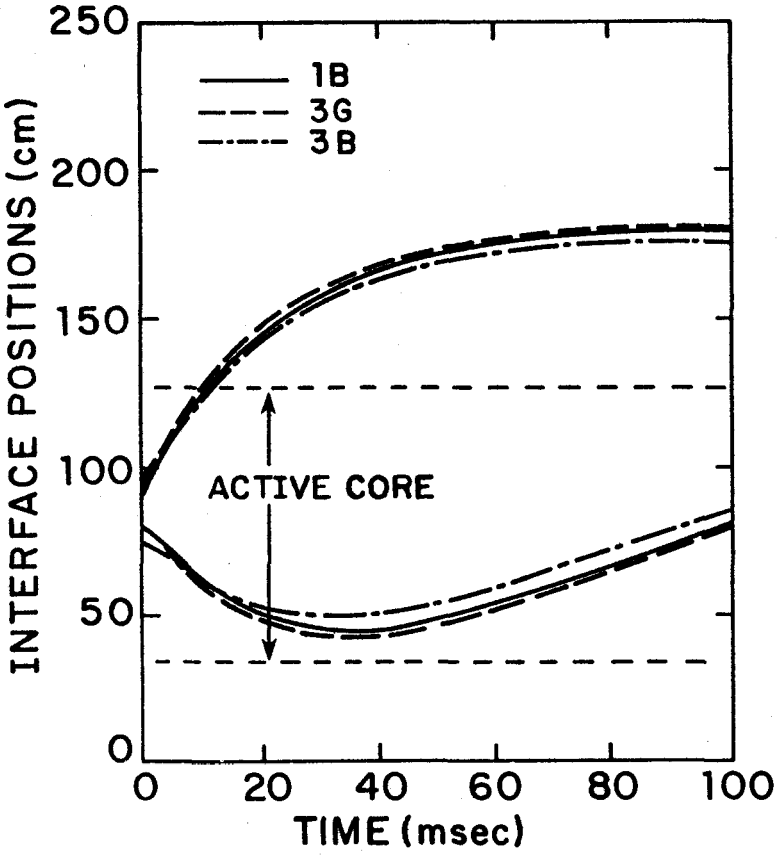

Figure 3.3 Effects of halving (Case 3G) and doubling (Case 3B) sodium masses from base value (Case 1B).

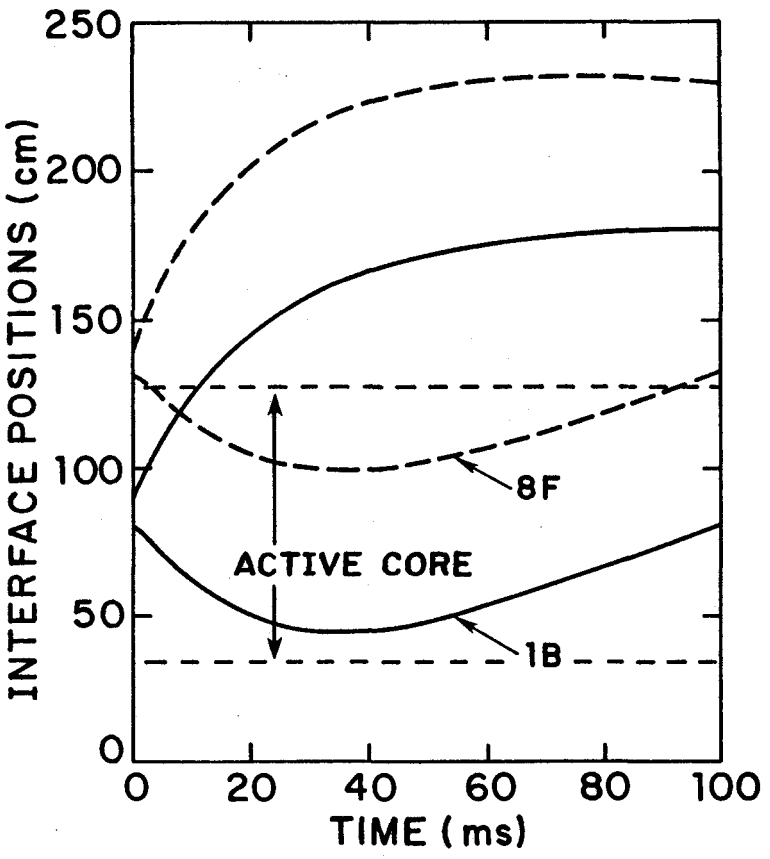

Figure 3.4 Demonstration that shifts in initial zone location serve only to correspondingly shift voiding pattern.

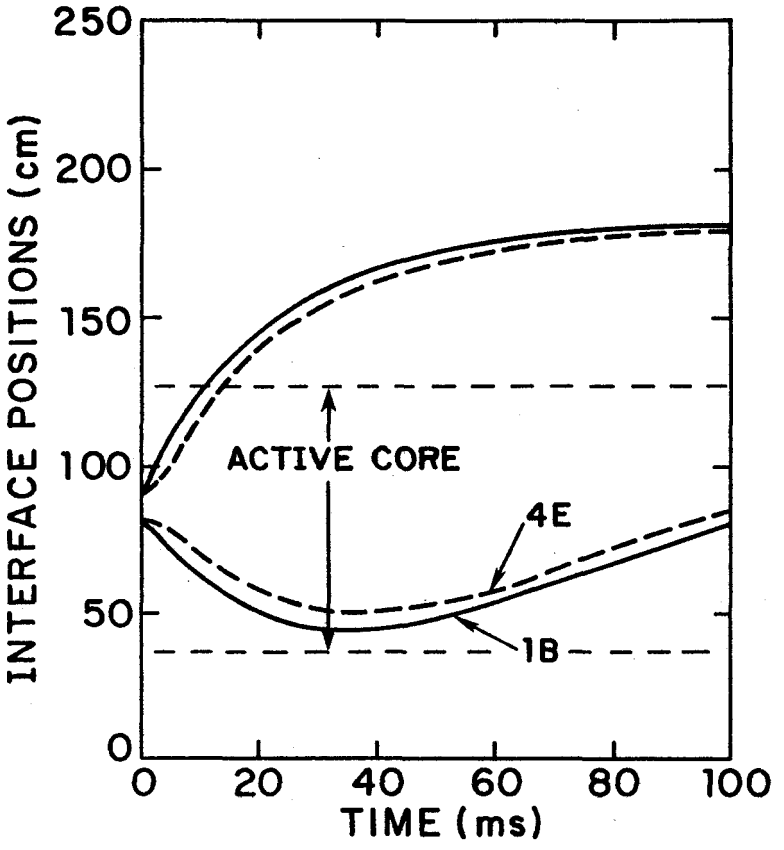

Figure 3.5 Mitigating effect of non-condensable gasses (Case 4E) on voiding history without gas (Case 1B).

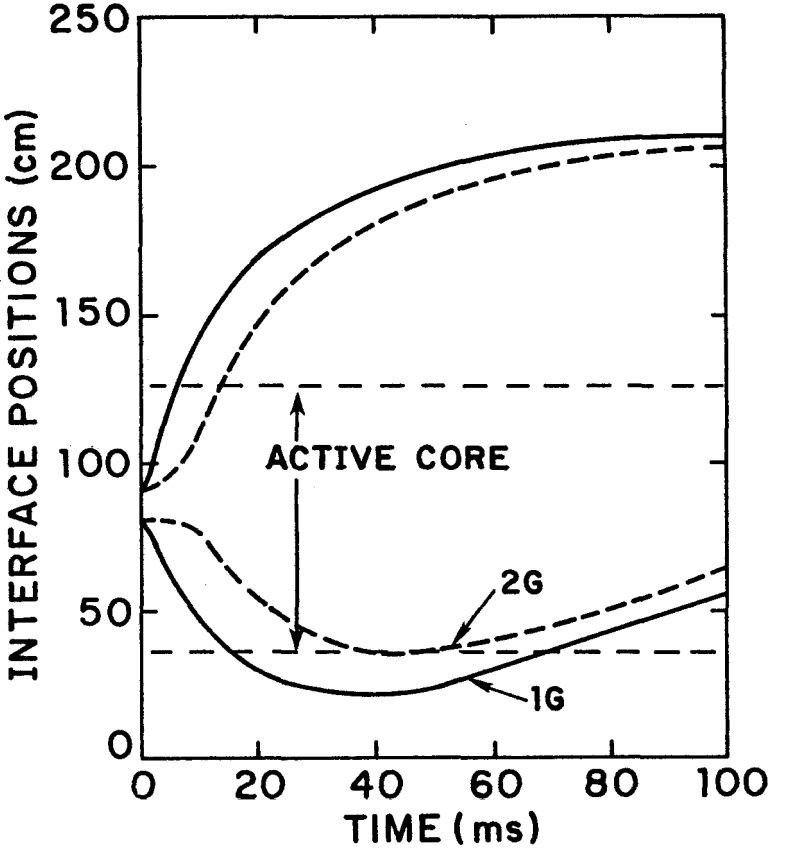

Figure 3.6 Effect of 0.01 s mixing time (Case 2G) compared to coherent mixing (Case 1G).

mixing times greater than 10 milliseconds were not considered. Results of studies showing only a shift in timing of the voiding for mixing times from zero to 5.0 milliseconds were reported in our second quarterly[1]; however, sodium-to-cladding heat transfer effects were not included in those calculations. Figure 3.6 compares case 1G (similar to 1B but twice the fuel mass, i.e. 6.4 g) with case 2G in which a linear addition of the same amount of fuel over 10 milliseconds was modelled. There is a detectable, although not order-of-magnitude, reduction in the extent of voiding in both time and space.

Other second order effects are produced by variations in initial fuel and sodium temperatures. Comparisons of these effects using 1B as a reference are not available; however, later runs which represented more closely our current judgement regarding likely FCI conditions are available. Figure 3.7 shows voiding histories for two runs whose initial parameters differed only in fuel temperature, one (BOL-3) set at 3750 K and the other (BOL-1) at 3500 K. The difference in voiding histories is barely noticeable. For comparisons of cases in which the initial sodium temperature was varied by 100 K, no differences in the voiding histories and only slight differences in peak FCI pressure were detectable.

3.5 Key Parameters

Parametric studies such as the ones described above in 3.4 led us to the expected conclusion that the governing parameters in FCI voiding in CRBR-type geometry are those which determine the ratio of the heat transfer rates from fuel to sodium and from sodium to cladding. Those parameters are fuel mass, fuel particle size, and zone-to-cladding heat transfer coefficient. The reference case 1B described in Section 3.4 demonstrated that 3 to 4 g of fuel per pin could produce significant long-term voiding if the particle diameter was 250 microns and the sodium-to-cladding heat transfer coefficient was 5.674 $W/cm^2 \cdot K$. The uncertainty in effective particle diameters and in heat transfer coefficients, especially for the latter in the presence of non-condensable gases, motivated studies such as those presented in Figure 3.8. There, the 1B results are compared with a case

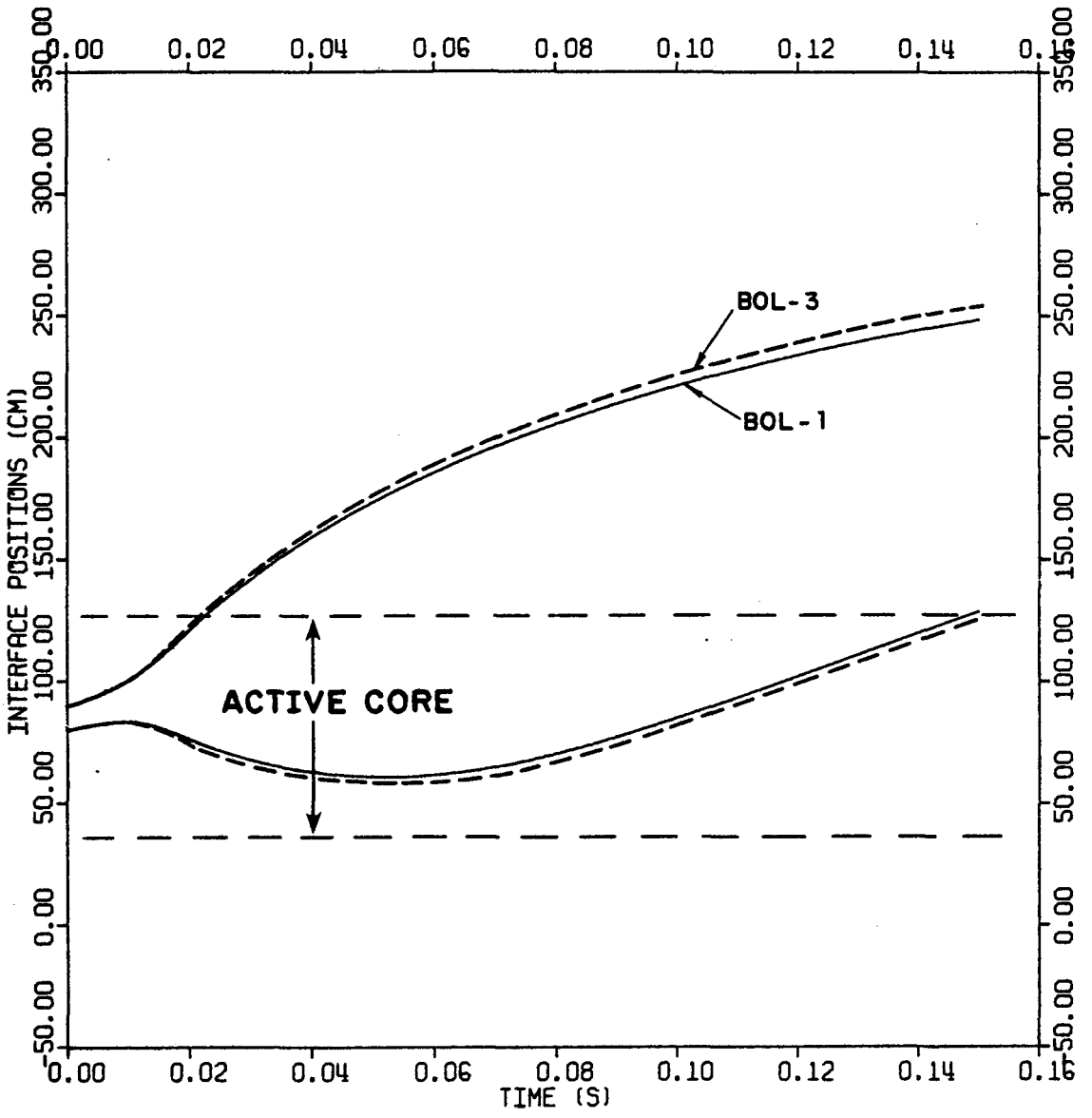

Figure 3.7 Demonstration that a variation in initial fuel temperature of 250 K (i.e. 3500 K for BOL-1 and 3750 K for BOL-3) has little impact on voiding histories.

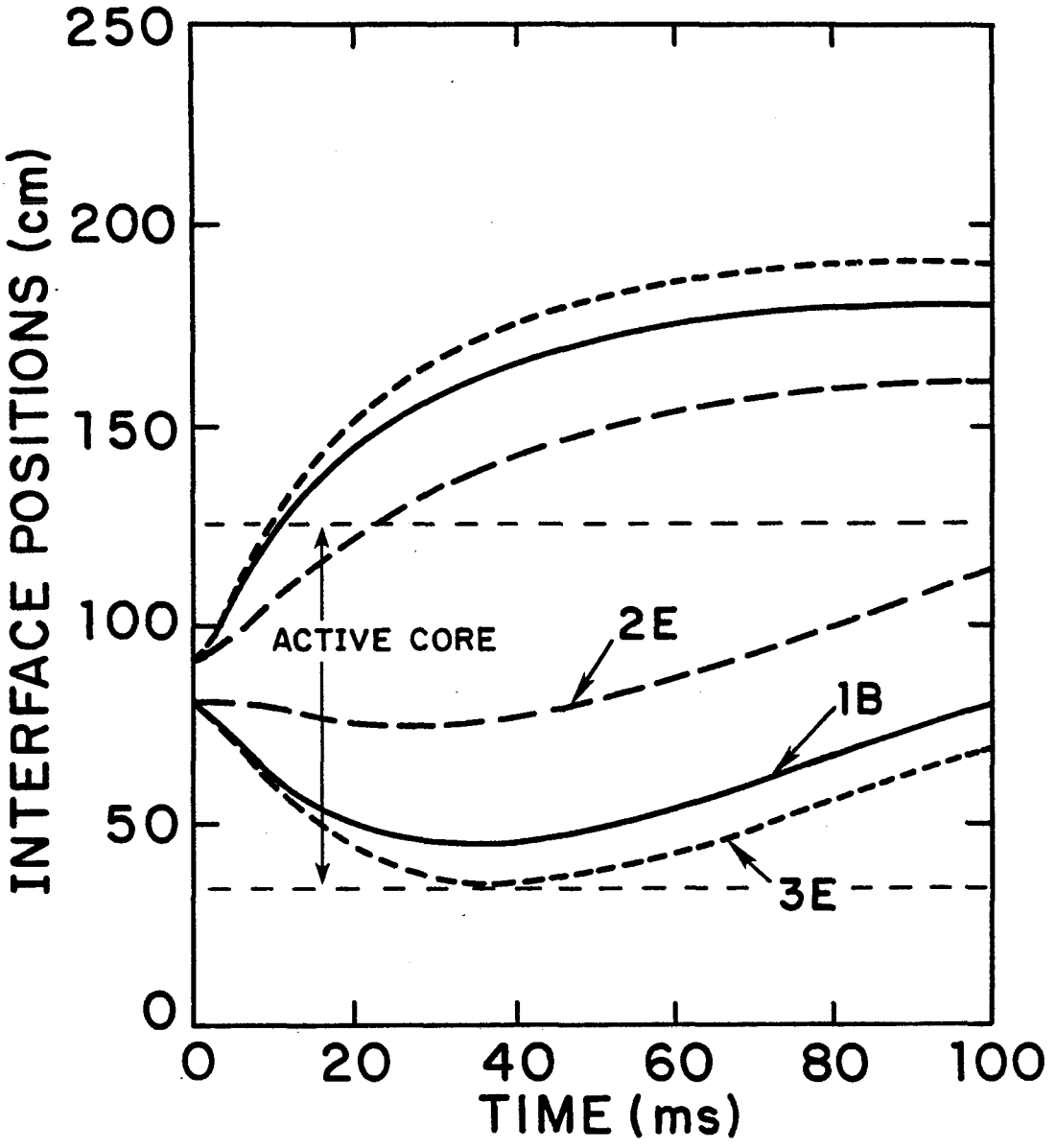

Figure 3.8 Effects on voiding history of doubling fuel particle size (Case 2E) or halving zone-to-cladding heat transfer coefficient (Case 3E) relative to Case 1B.

in which the only change from 1B was a doubling of particle size (Case 2E). The voiding is distinctly milder for this 512 micron diameter particle size. Since the fuel-to-sodium heat transfer rates at low void fractions scale inversely to the square of the radius but proportionally to the mass of fuel, we note that approximately four times the mass of fuel would be needed to offset the larger particle size.

Also in Figure 3.8, we see the results from a case in which the only change from 1B input was halving the sodium-to-cladding heat transfer coefficient (Case 3E). The increase in vigor of voiding for 3E over 1B is, as we would expect based on the arguments of Section 2.1, not as dramatic as the decrease in voiding for 2E relative to 1B. To offset a factor of two increase in particle size we would need a factor of four decrease in sodium-to-cladding heat transfer coefficient or a combination of changes such as halving the heat transfer coefficient and doubling the mass of fuel.

Once an acceptable range of particle sizes and sodium-to-cladding heat transfer coefficients are selected (see Appendix B), the minimum fuel masses required for large-scale voiding can then be determined (consistent with modeling of 2D or noncoherence effects discussed in Section 4). The preceding statement applies to initiation of voiding and the early, rapid growth of the FCI zone. However, another key parameter was identified relatively late in the contract work which appears to be crucial to maintaining extensive voiding in our UVAFCI calculations. That factor is the initial cladding temperature, T_{ci}. As indicated in Section 2.2, the cladding represents a large heat sink. This sink is so large that for long-term voiding (e.g. > ~ 30 milliseconds) the sodium temperature follows the cladding temperature very closely. This means that differences in initial cladding temperature produce corresponding differences in two-phase sodium temperatures and therefore differences in sodium vapor pressures for long-term voiding.

The phenomenon discussed above is illustrated by the voiding and pressure histories of Figures 3.9 and 3.10. The results presented in those figures are from two runs, BOL-8 and BOL-9, for which the input

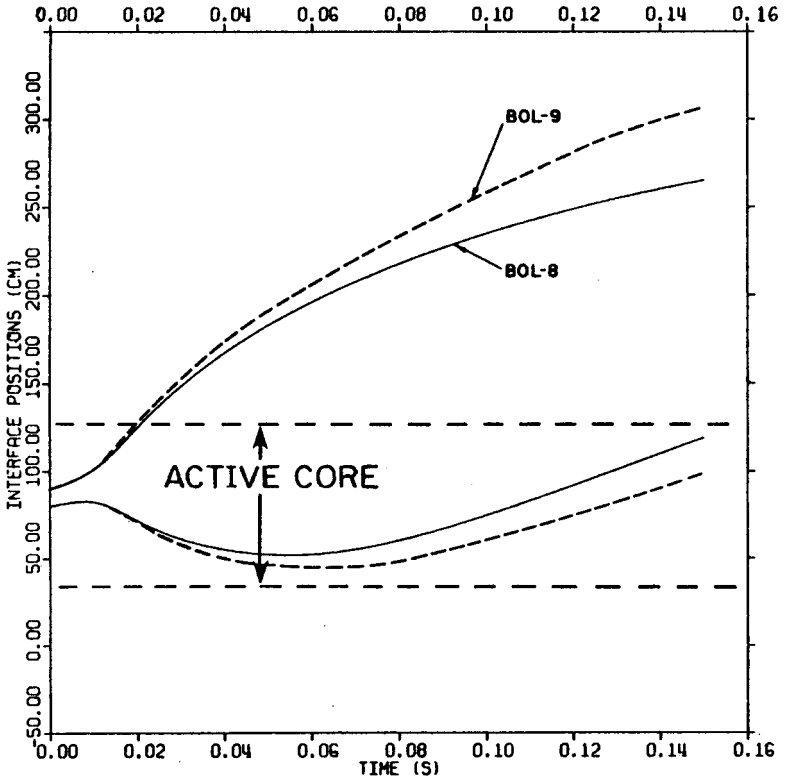

Figure 3.9 Dependence of voiding history on assumed initial cladding temperature (1100 K for BOL-8, 1200 K for BOL-9).

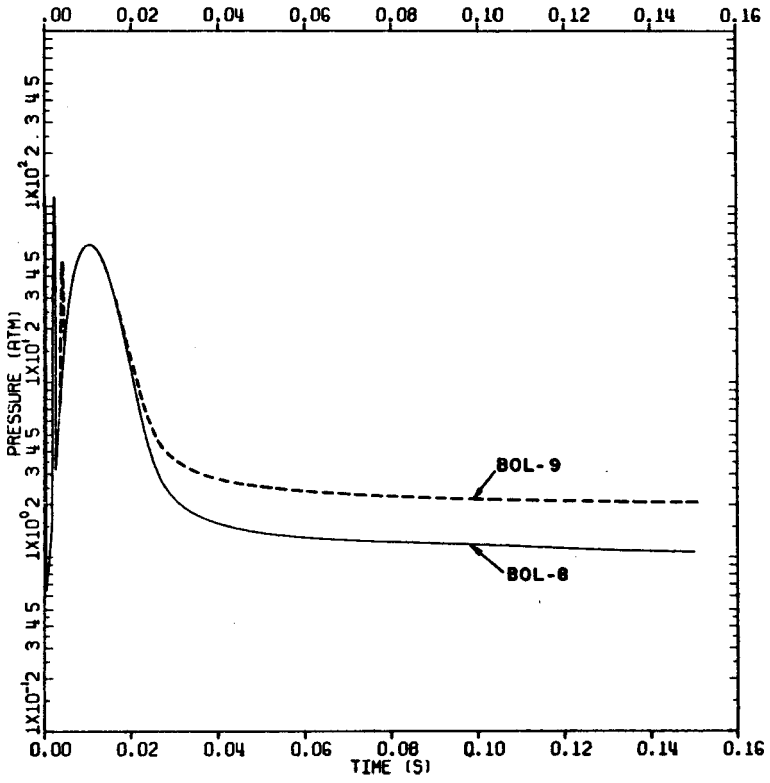

Figure 3.10 Dependence of pressure history on assumed initial cladding temperature (1100 K for BOL-8, 1200 K for BOL-9).

data were identical except for the initial cladding temperature. The important common input parameters are shown below.

Interacting masses

fuel = 4.8 g

sodium = 1.6 g

Initial temperatures

fuel = 3900 K

sodium = 1100 K

Fuel particle diameter = 632 microns

Sodium-to-cladding heat transfer coefficient = 5.674 $W/cm^2 \cdot K$

Mixing time = 0.005 s

Cases BOL-8 and BOL-9 had initial cladding temperatures of 1100 K and 1200 K respectively. The increased extent of overall voiding and higher zone pressures for BOL-9 for time $\geq$ 30 milliseconds are significant.

The zone pressures at long times are quite consistent with the differences in the initial cladding temperatures; the sodium in the BOL-9 case is about 100 K higher in temperature than for BOL-8. The short table below presents sodium temperatures and pressure histories confirming this statement.

Table 3.1

Zone Temperature and Pressure Histories as a Function of Initial Cladding Temperature, T_{ci}

Time (msec)	BOL-8 (T_{ci} = 1100 K)		BOL-9 (T_{ci} = 1200 K)	
	Temp (K)	Press (atm)	Temp (K)	Press (atm)
10.1	1920	60.0	1936	63.1
20.1	1511	11.5	1547	13.8
29.5	1253	2.26	1326	3.85
39.5	1207	1.58	1289	2.97
49.5	1191	1.38	1275	2.68
59.5	1184	1.29	1268	2.54
69.5	1180	1.25	1264	2.45
79.5	1177	1.22	1260	2.40
99.5	1173	1.17	1256	2.32
119.5	1167	1.12	1251	2.24
150.0	1162	1.07	1251	2.24

The effect of zone pressures will, of course, be even more dramatic for values of T_{ci} greater than 1200 K. For case BOL-10, which was identical in set-up to BOL-8 except T_{ci} = 1300 K, the values of zone sodium temperature and pressure at 150 msec were 1342 K and 4.26 atm.

The calculations discussed above assume uniform initial cladding temperatures, but the cladding temperature is allowed to vary axially and with time during the voiding. (Note that published PLUTO calculations[5] which model the voiding assume a constant as well as uniform initial cladding temperature.) It appears important to correctly model the actual cladding temperature at pin failure, as in SAS[6].

It became clear that for our parametric calculations there are four key parameters which will control the voiding dynamics:

1. mass of fuel involved
2. size of fuel particles
3. FCI zone sodium-to-cladding heat transfer coefficient
4. initial cladding temperature

It is the proper selection of a combination of these parameters which will correspond to determination of the minimum requirements for large-scale voiding. Before a discussion of that selection process is presented (Section 5), we will address two other important factors in subassembly voiding: 2D and/or non-coherence effects.

REFERENCES
(Section 3)

1. C. A. Erdman, M. B. Johnson, and A. B. Reynolds, Quarterly Progress Report for Oct. 1, 1975-Dec. 31, 1975, NRC Contract No. AT(49-24)-0158, University of Virginia.

2. C. A. Erdman, M. B. Johnson, and A. B. Reynolds, Quarterly Progress Report for Jan. 1, 1976-March 31, 1976, NRC Contract No. AT(49-24)-0158, University of Virginia.

3. T. C. Chawla et al., "The Rate of Coolant Recovery Following Rapid Release of Fission Gas from a Postulated Multiple Pin Failure in an LMFBR Assembly," TANS, 20, 315 (June 1975).

4. P. M. Haas, "Improved Modeling of the Fuel-Coolant Interaction in the Hypothetical Core-Disruptive Accident for the Liquid-Metal Fast Breeder Reactor," Ph.D. Dissertation, Nuclear Engineering Department, University of Virginia, pp. 114-136 (1974).

5. H. U. Wider, " An Improved Analysis of Fuel Motion During an Over-power Excursion," Ph.D. Dissertation, Nuclear Engineering, Northwestern University (June 1974).

6. M. G. Stevenson et al., "Current Status and Experimental Basis of the SAS LMFBR Accident Analysis Code," Proc. ANS Fast Reactor Safety Conf., Beverly Hills, California, CONF-740401, pp. 1303-1321 (April 1974).

4. 2D AND/OR NON-COHERENCE EFFECTS

Our interest in the two-dimensional aspects of subassembly voiding were directed not so much toward obtaining exact spatial details of voiding in the radial direction as in determinations of the effect of the 2D nature of the voiding on the time-scale and extent of large-scale voiding.

Early in the contract period[1] we concluded that the 2D aspects of voiding - for gas release or FCI - are probably not important except as they relate to non-coherence in pin failure and condensation on duct walls and intact pins during an FCI. Once the voided region has extended one or two equivalent subassembly diameters along the subassembly, any 2D flow patterns are not likely to have a significant effect on the overall voiding dynamics.

The rapid transition to a 1D analysis can be argued as follows: the bubble (FCI or gas) may initially be concentrated radially in the center of the subassembly with liquid sodium (still moving upward but with a reduced speed) between the bubble and the duct walls. The bubble may be assumed to have a uniform pressure based on the relative inertias of the bubble and constraining slugs. This relatively uniform pressure insures that the liquid sodium in the annular region between the bubble and the duct walls will not be rapidly accelerated axially due to pressure forces. However, the upper and lower constraining slugs of sodium will be accelerated by the bubble pressure, producing column separation within the annular regions at both the top and the bottom of the bubble.

Assuming that no separation were to occur before reversal of the lower sodium slug, the length of the annular region at the time of reversal would be of the order of a few centimeters for large-scale gas releases from high-burnup pins and perhaps the order of 10 cm for FCI-induced voiding. Further assuming initial slug accelerations (both upward and downward) of 3×10^3 m/sec^2 (from $\Delta P/L\rho \sim 40$ atm/4 ft $\times$ .8 g/cc = 4×10^6 Pa/1.3 m $\times$ 800 Kg/m^3) for this early, high-pressure stage, the bubble length would grow 30 cm in 10 msec. This indicates that the expanding bubble would quickly fill the subassembly cross section at the

slug interfaces and that the sodium remaining in the failure region would simply mix into the bubble. This would be unimportant for gas release in terms of secondary failures. For an FCI bubble, the amount of sodium in this annular region could be somewhat larger. This sodium would eventually act as a heat sink but would initially tend to move above the failure sites and would probably not cause a significant change in the axial location of secondary failures.

Based on the above discussion, our concerns with the 2D aspects of voiding shifted toward simulation of non-coherence in pin failure. In particular we were interested in the failure of only the center 50% of the pins within a given subassembly.

The major effect of failing only half the pins within a given subassembly would be to effectively increase both the flow area and condensing surfaces available to the expanding FCI zone in our single-channel UVAFCI model. This can be simulated within the model simply by halving the masses of both fuel and sodium involved in the FCI. Thus the modeled FCI zone is effectively smeared radially across the subassembly, and the additional cold structure surfaces are made available as a heat sink.

This simulation technique probably over-emphasizes the ameliorating effects of non-coherence in the initial voiding phases, because the additional heat loss surfaces are not instantaneously available at pin failure. Moreover, the voiding induced by the central 50% of the pins will contribute to failure of the outer pins by reducing heat removal capabilities while simultaneously contributing positive reactivity to drive power up. When the outer pins fail, their contribution of molten fuel or fission gases to the subassembly voiding should be considered. This was not done for cases discussed below.

Simulation of failure of 50% of the pins is illustrated in Figure 4.1, which is partially a reproduction from our third quarterly[2]. The voiding history for the reference case 1B (described in Section 3.4 of this report) is plotted against 4B, which utilized only half the amounts of fuel and sodium in the interaction zone as did 1B. Our comments in Section 3.4 on the second order effects of varying sodium mass would

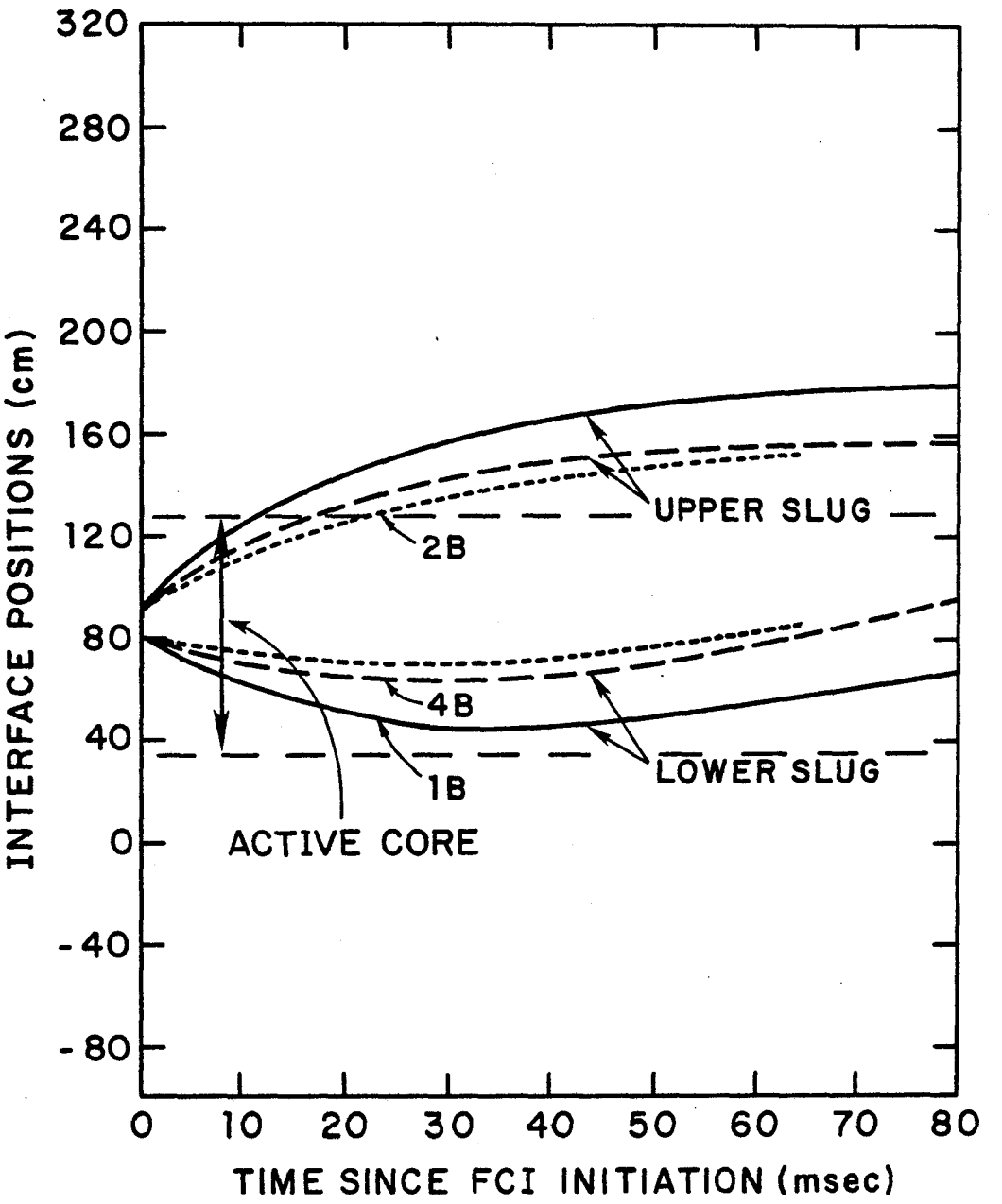

Figure 4.1 Simulation of 50% failure (Case 4B) by halving fuel and sodium masses relative to Case 1B. Also, effect of halving only the fuel mass is illustrated (Case 2B).

suggest that essentially all the difference in cases 1B and 4B was due to the halving of fuel mass in going from 1B to 4B. To confirm this suggestion, the results of case 2B, which is identical to 1B except for a halving of the mass of fuel involved, are also shown in Figure 4.1. The comparison of the three cases together does show that most of the difference in cases 1B and 4B was due to differences in fuel mass, but the reduction in the amount of sodium available as a quenching agent is detectable and should be included in any 50% failure studies.

REFERENCES
(Section 4)

1. C. A. Erdman and A. B. Reynolds, Quarterly Progress Report for July 1, 1975-Sept. 30, 1975, NRC Contract No. AT(49-24)-0158, University of Virginia.

2. C. A. Erdman, M. B. Johnson, and A. B. Reynolds, Quarterly Progress Report for Jan. 1, 1976-March 31, 1976, NRC Contract No. AT(49-24)-0158, University of Virginia.

5. PARAMETRIC STUDIES - MINIMUM REQUIREMENTS FOR EXTENSIVE VOIDING IN THE CLASSICAL TOP

The work discussed in Sections 2, 3, and 4 provided a basis for studies on the minimum requirements for voiding. We indicated in Section 3.5 that four major or key parameters needed to be considered, but we still needed reasonable values for other pin failure conditions. Most of our TOP failure conditions were obtained from personnel in the Fast Reactor Safety Division of Brookhaven National Laboratory. In particular we received aid and information from P. M. Haas, T. P. Henry, T. Ginsberg, and J. G. Refling.

Although a wide range of burnup conditions, initiating ramp rates, and failure criteria can be considered in characterizing pin failure conditions, we initially chose to simplify selection of conditions in the following ways. We looked only at ramp rates of the order of 50¢/sec or less, with emphasis on ramp rates of the order of 10¢/sec. Rather than considering an infinite spectrum of burnup conditions, we considered only beginning-of-life versus burned pins, where "burned" implies at least one cycle of operation. Failure conditions for burned pins were generally based on the burst pressure criterion as modified by the GE cracking model[1]. For fresh pins, a high melt fraction failure criterion was sometimes employed in the data base we examined.

The net result of this search for failure conditions was the selection of two sets of base conditions at failure: beginning-of-life and burned, with the major differences in the sets of conditions being the mass of fission gas present; the molten fuel, sodium, and cladding temperatures; and the mass of molten fuel available in the pin. The failure conditions used in determining initial FCI parameters for each of the base conditions are described in the appropriate section below.

5.1 Beginning-of-Life (BOL) Studies

For BOL pin failures, we typically expect high average temperatures in molten fuel and a large molten fuel mass. (The mass of molten fuel is an important quantity in that we are interested in determining whether or not a small fraction of this available molten fuel will

produce extensive voiding.) The BNL runs gave us average molten fuel temperatures in the range of 3650 to 4100 K, depending on ramp rates and failure criteria. We took a value of 3900 K for most cases. (Note again the second order effect of fuel temperature as discussed in Section 3.4.)

Molten fuel masses per pin at failure ranged from about 70 to 100 g. Molten fuel masses used in our final BOL calculations were less than 5.0 g; thus only a small fraction of the molten fuel inventory was used. This fact is important because the driving forces for fuel ejection may drop rapidly following pin failure if small quantities of manufacturing or fill gases rather than fuel vapor pressure provide the driving force. Based on fuel ejection rates discussed in 3.4 and the 5 g upper limit on total fuel ejection, a mixing time of 5 milliseconds was used in most BOL calculations.

Sodium temperatures at the failure site depend on the failure location in addition to other obvious factors. For near-midplane failures, temperatures ranged from 1000 K to 1200 K; a value of 1100 K was used in most of our BOL runs. Values as high as 1500 K could be justified based on failure near the top of the active core, and such high values should lead to more sustained voiding. However, no initial sodium temperatures over 1200 K were examined.

The mass of sodium involved was taken as 1.6 g for most BOL and burned pin cases, based on 10 cm of channel length. The selection of this 10 cm length was discussed briefly in our second quarterly[2], but a strong justification is not available. However, PLUTO[3] runs made at UVA and SAS runs at BNL do support this mass of sodium as being typical. Moreover, for long-term voiding, we see a relative insensitivity to the sodium mass as discussed several times earlier in this report, including Section 3.4.

The nominal values for the various parameters just discussed are summarized in the table below.

Table 5.I

Nominal Values for Second-Order-Effect Parameters (BOL Runs)

Initial temperatures

fuel = 3900 K
sodium = 1100 K

Sodium mass = 1.6 g

Mixing time = 0.005 s

Initial interface locations
(relative to bottom of lower blanket)

upper = 90 cm
lower = 80 cm

The next step was to select nominal values for the key parameters. We looked on minimum fuel mass needed as being a dependent variable which was determined by the values selected for particle size; sodium-to-cladding heat transfer coefficient, h; and initial cladding temperatures, T_{ci}. A value of 5.674 W/cm^2•K for h was used in all of the later BOL runs. As indicated in Reference 4 and Appendix B, this value of h could be interpreted as maximizing the benefits of the heat sink, but our cladding treatment included a consideration of conduction limited heat transfer within the cladding, which reduced the effective value of h. (For the burned pin runs, lower values of h were chosen based on the presence of non-condensable gases.)

The nominal fuel particle diameter was taken as 200 microns. This is consistent with many reported fuel fragmentation results on mass-mean diameters (e.g. Reference 5), and indeed a smaller diameter could be argued on the basis of Sauter-mean diameters (average volume to surface ratio).

The nominal T_{ci} was taken as 1200 K, based on the cladding being initially hotter than the sodium at the failure site. In retrospect, that should not have been the criterion, since T_{ci} should be representative of all the regions of cladding which will be exposed to the FCI zone and not just the cladding at the failure location. However, while cladding low in the core will exhibit lower

initial temperatures than 1200 K, cladding near the top of the core will have temperatures upward of 1600 K. Thus the selection of 1200 K may be acceptable.

With the nominal values for h, T_{ci}, and particle diameter as discussed above, a value of 4.8 g for the fuel mass is sufficient to produce extensive, long-term voiding in the BOL situation. The nominal values for the key parameters are listed again below.

Table 5.2

Nominal Values for Key Parameters (BOL Runs)

Fuel mass = 4.8 g

Particle diameter = 200 microns

Sodium-to-cladding heat transfer coefficient = 5.674 $W/cm^2 \cdot K$

Initial cladding temperature = 1200 K

The combination of nominal values from Tables 5.1 and 5.2 were used in a UVAFCI run designated BOL-9H, for which voiding and zone pressure histories are presented in Figures 5.1 and 5.2. From Figure 5.1 we see that the voiding is quite extensive in both space and time. The lower sodium slug does not start returning until about 60 milliseconds after FCI initiation. Moreover another 60 milliseconds later (at 120 milliseconds), the lower slug was still 35 cm below its original location. This voiding is sufficient to set up the scenario of late-ejected fuel (after first 10 to 20 milliseconds) entering a partially voided channel and therefore not being susceptible to easy fragmentation and sweepout.

Regarding Figure 5.2, the early, large pressure spikes are due to the pure inertial constraint utilized in the calculation which permits reentry into single phase as fuel is added and causes the very large initial spike. Note, however, that the impulse associated with those spikes is unimportant to the long-term voiding.

If the failure of only half of the pins is simulated (BOL-12H) the voiding is still extensive. The voiding history from run BOL-12H is shown in Figure 5.3 along with that of BOL 9H. The input for BOL-12H was identical to that for BOL-9H except that the masses of fuel and sodium involved were halved.* Note that the lower sodium slug starts back

*Table C.2 of Appendix C summarizes parameter values for all BOL runs discussed here.

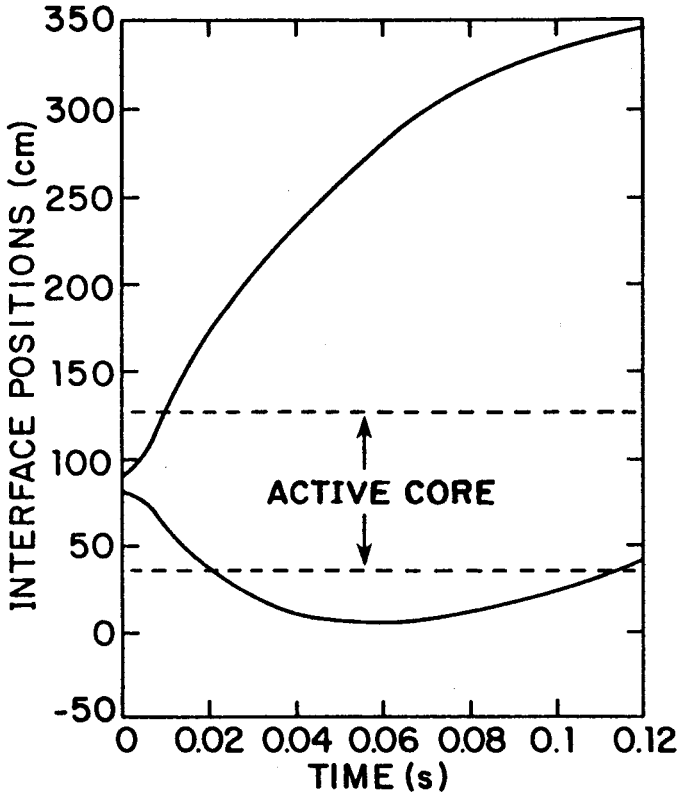

Figure 5.1 Voiding history for Case BOL-9H, which utilized nominal BOL parameter values and 4.8 g of fuel.

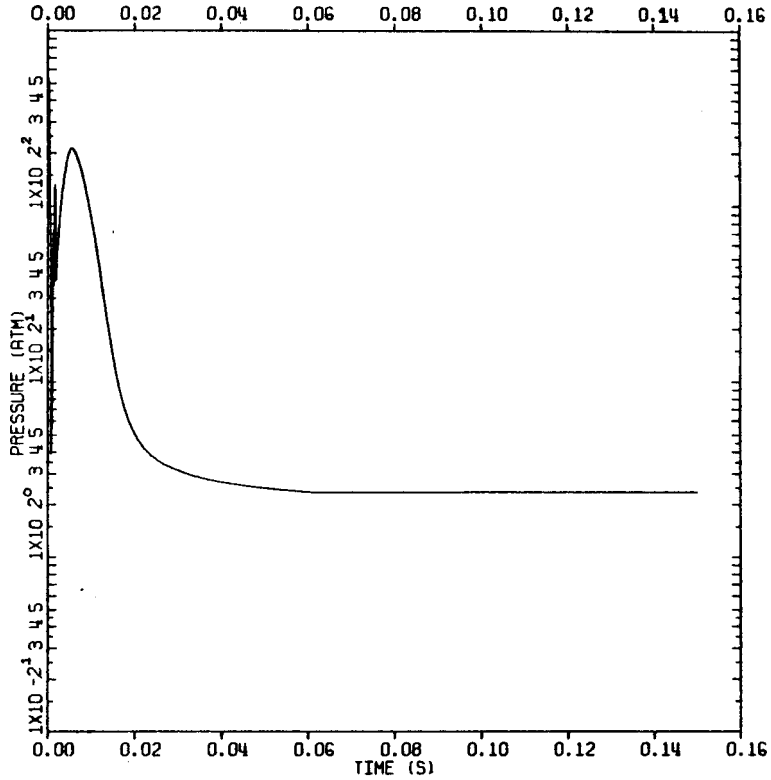

Figure 5.2 Pressure history for Case BOL-9H, which utilized nominal BOL parameter values and 4.8 g of fuel.

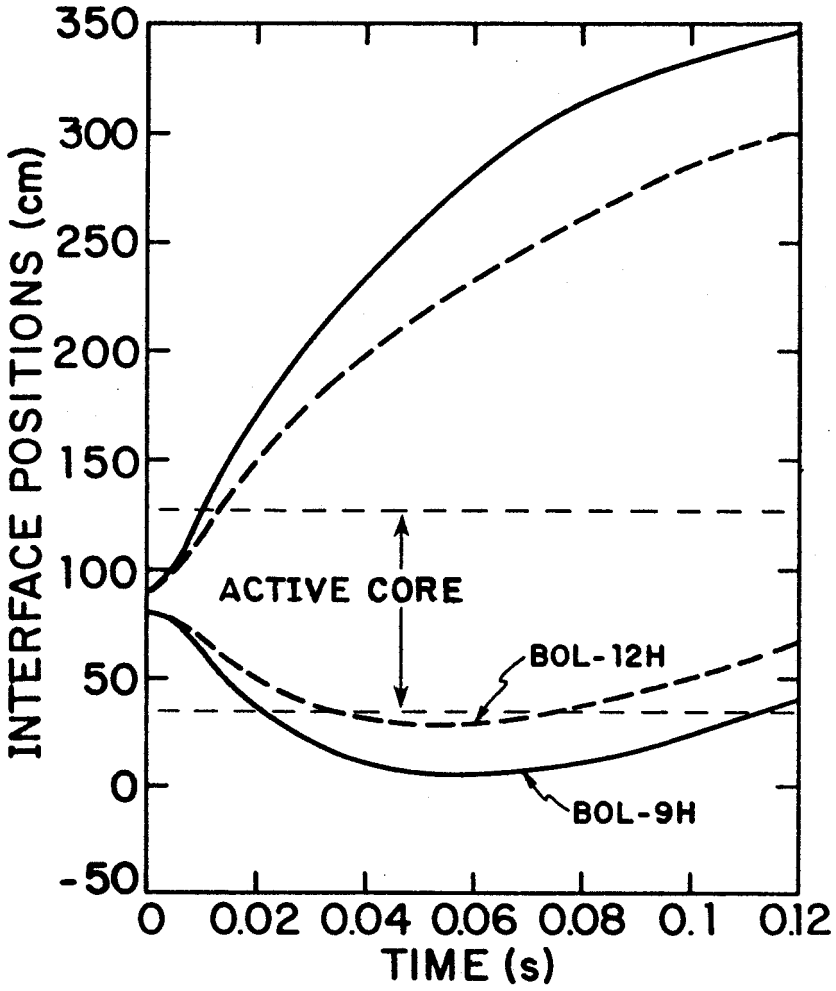

Figure 5.3 Simulation of failure of 50% of the pins (Case BOL-12H) compared to 100% failure (Case BOL-9H).

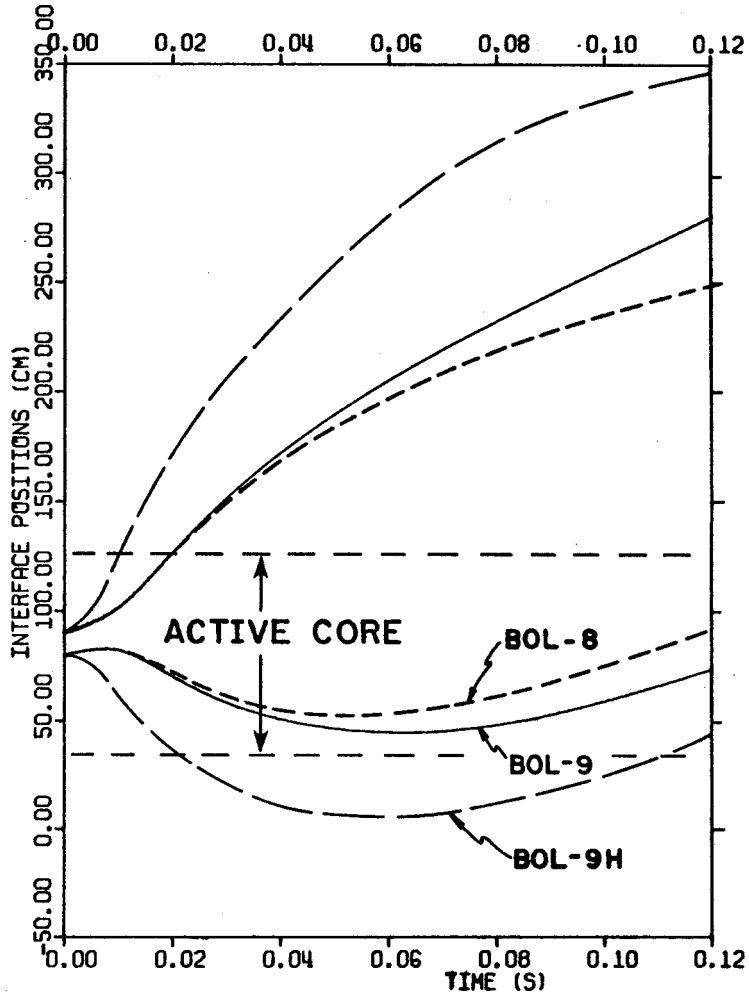

Figure 5.4 Effect of increased particle size (Case BOL-9) and of the combination of increased particle size and lower initial cladding temperature (Case BOL-8) on voiding histories.

up earlier than for BOL-9H (50 msec vs. 60 msec), but is still below its initial location at 120 msec.

The next two figures give comparisons of the BOL-9H run with other runs in which key perameters were varied. Figure 5.4 shows results of BOL-9, for which the particle diameter was 3.16 times the nominal value of 200 microns, i.e. the particle diameter was 632 microns. Also shown is the voiding history for BOL-8, in which the large 632 micron particle was assumed along with lower initial cladding temperature (1100 K in BOL-8 vs. 1200 K in BOL-9H and BOL-9). Even with the large particles used in the BOL-9 case, the lower slug does not return to its initial position by 120 msec after FCI initiation. Moreover, the results for the BOL-8 case, which assumed the lower cladding temperature in addition to the large particle size, showed that the lower slug had not regained its initial position at 100 msec after FCI initiation.

In Figure 5.5 we see the effect of increasing the initial cladding temperature. Input for run BOL-10H differed from BOL-9H only in the value of T_{ci}, which was 1300 K for BOL-10H vs. 1200 K for BOL-9H. The voiding in BOL-10H actually extended down below the pin bundle and into the shield region.

It would be possible to give many examples of cases for which voiding was much more or much less vigorous than for BOL-9H; however, it is clear that to eliminate extensive voiding we would have to assume values for single key parameters that are far from the nominal values or else have two or three of the key parameters varied together in the desired direction. It also seems clear that the parameter values of Tables 5.1 and 5.2 will indeed give extensive voiding and that the minimum requirements for extensive voiding would be somewhat less than those indicated in the tables. Certainly the required mass of ejected molten fuel per failed pin can be argued to be less than 5.0 g for coherent failure of 50% or more of the pins in a single subassembly, and this mass will be significantly less than 10 % of the molten mass available at pin failure.

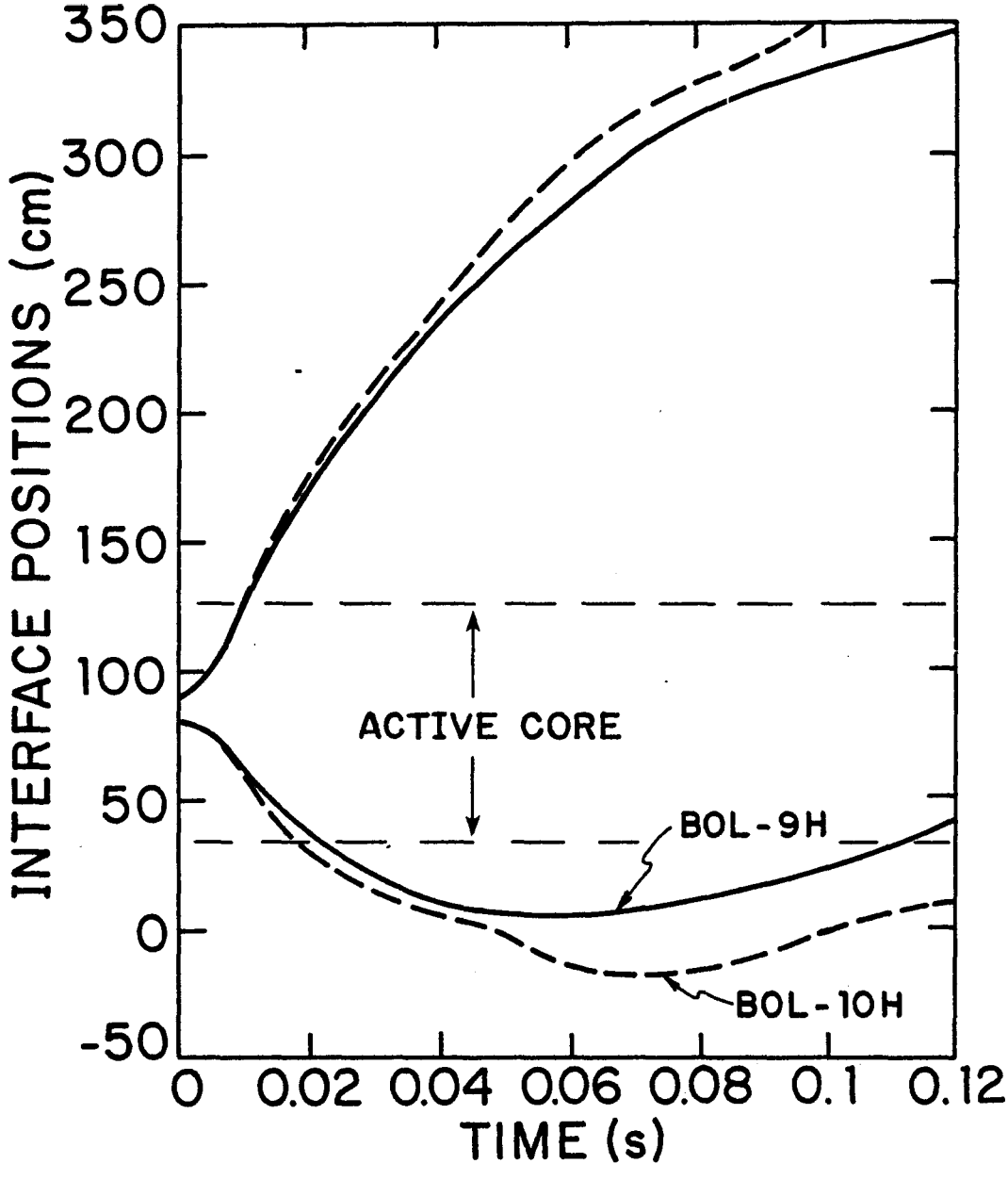

Figure 5.5 Effect on voiding history of increasing T_{ci} from 1200 K (Case BOL-9H) to 1300 K (Case BOL-10H).

5.2 Burned-Fuel Studies

As indicated in Section 5.1, the runs mocking up burned-fuel subassemblies differed in failure conditions from the BOL runs in terms of mass of fission gas present, temperatures (fuel, sodium, and cladding), and mass of molten fuel available. Otherwise the general modeling was similar for burned and BOL pins. We will consider the three principal areas of difference between BOL and burned-pin failure conditions stated above individually, even though the three areas are really related. The relationship can be simply stated as follows: the presence of significant quantities of fission gasses tends to produce early failures in burned pins relative to BOL pins, and the earlier failures translate to lower temperatures and smaller melt fractions at failure.

For mild FCI's following failure the fission gas may be a major factor in pressurization of the coolant channel; however, the role of the fission gas following pin failure is relatively unimportant to direct generation of pressures if a vigorous FCI occurs. The important roles of the gas in a vigorous FCI are ejection of fuel from the pin and potential reduction of heat transfer from the FCI zone sodium to the cladding and structure. In Appendix B the arguments for selection of a reduced heat transfer coefficient due to the gas are presented. The importance of this coefficient to calculated voiding results is discussed later in this section.

The lower temperatures of fuel, sodium, and cladding at failure tend to reduce the voiding, but these reductions in temperature are overpowered by reductions in the sodium-to-cladding heat transfer coefficient. Once again we relied mainly on BNL SAS runs for failure conditions. Molten fuel temperatures in the central cavity averaged from 3325 to 3625 K. We used a value of 3500 K for most burned-pin (usually labeled BURN) runs. Masses of molten fuel at failure varied from about 45 to 80 g, depending again on ramp rates, exact burnup, and gas release model used. These molten fuel masses were slightly lower than for BOL pins, but provided a large inventory of molten fuel available for secondary ejection, even after ejection of an initial 5 to 10 g.

Sodium temperatures at the fuel axial midplane varied only a few tens of degrees, and a representative value of 1000 K was used for the BURN series of runs. Table 5.3 below summarizes the nominal values of the various parameters for which credible variations were found to have little effect on the FCI voiding.

Table 5.3

Nominal Values for Second-Order-Effect Parameters (BURN Runs)

Initial temperatures

fuel = 3500 K
sodium = 1000 K

Sodium mass = 1.6 g

Mixing time = 0.010 s

Initial interface locations

upper = 90 cm
lower = 80 cm

The longer mixing time (as compared to 0.005 s for BOL runs) is based on the idea that the driving force for fuel ejection will be more sustained in burned pins than BOL pins if gas (fission, fill, or manufacturing) is the driving force in both instances. Continuing with that argument, larger masses of ejected fuel could be considered for the BURN series of runs. Initially then we felt it would be reasonable to consider the order of 9.6 g/pin from burned pins vs. 4.8 g/pin for BOL pins. As will be illustrated later, even BURN runs which used 4.8 g/pin showed extensive voiding due to the nominal value of 1.891 $W/cm^2 \cdot K$ selected for the sodium-to-cladding heat transfer coefficient, h. This value of h is only one-third of the nominal value for BOL runs.

As in the BOL nominal case, a particle diameter of 200 microns was assumed for the nominal BURN case. The remaining key parameter, initial cladding temperature, T_{ci} was assigned a value of 1100 K (100 K above the initial sodium temperature) to be consistent with the nominal cladding temperature in the BOL cases. The nominal values for all the key parameters are shown in Table 5.4 below.

Table 5.4

Nominal Values for Key Parameters (BURN Runs)

Fuel mass = 9.6 g

Particle diameter = 200 microns

Sodium-to-cladding heat transfer coefficient = 1.891 $W/cm^2 \cdot K$

Initial cladding temperature = 1100 K

The BURN run which utilized the values of Tables 5.3 and 5.4 was designated BURN-5H. The voiding and pressure histories for BURN-5H are shown in Figures 5.6 and 5.7. The initial voiding is extremely vigorous, with downward voiding extending well down into the shield-orifice region. The early pressures are very high even after reaching two-phase, but ultimately (times > 40 msec) the two-phase pressure is controlled by heat transfer to the cladding.

It is obvious from Figures 5.6 and 5.7 that BURN-5H utilized much more than the minimum requirements for large-scale voiding. Therefore, key parameters were varied separately to see how each might reduce the voiding to borderline magnitudes. The first such variation is depicted in Figure 5.8, which compares voiding histories for BURN-5H and BURN-9. BURN-9 used input parameters* identical to BURN-5H except for the choice of sodium-to-cladding heat transfer coefficient, h. For BURN-9, a value of 5.674 $W/cm^2 \cdot K$ was used. The voiding for BURN-9 is much milder than for BURN-5H at intermediate times, after heat transfer to the cladding becomes important but before it dominates. However, at 100 msec after FCI initiation, the lower interface positions are identical. This is primarily because the cases used identical initial fuel masses and cladding temperatures. The FCI zone pressures for BURN-5H and BURN-9 (no comparison shown) are similar at long times as would be expected, even though the BURN-9 pressures are lower for intermediate times.

The effect of increasing particle diameter by the factor of $\sqrt{10}$ (reduction in fuel-to-sodium heat transfer coefficient by factor of 10) is illustrated by Figure 5.9. Run BURN-5 assumed 632 micron diameter particles. Otherwise the input parameters were identical to BURN-5H. The reduction in voiding extent is only slightly greater than that for

*Table C.3 of Appendix C summarizes parameter values for all runs discussed here.

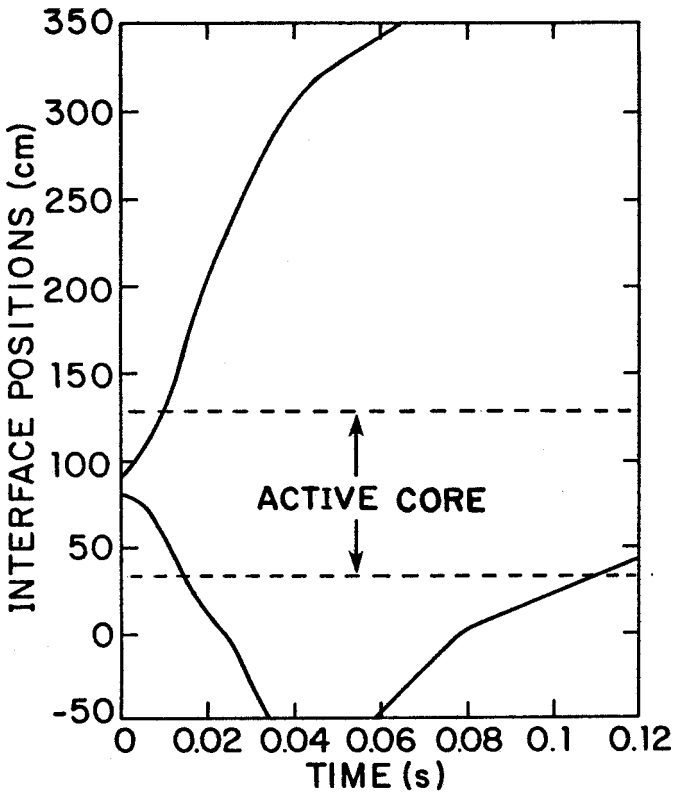

Figure 5.6 Voiding history for Case BURN--5H, which utilized nominal BURN parameter values and 9.6 g of fuel.

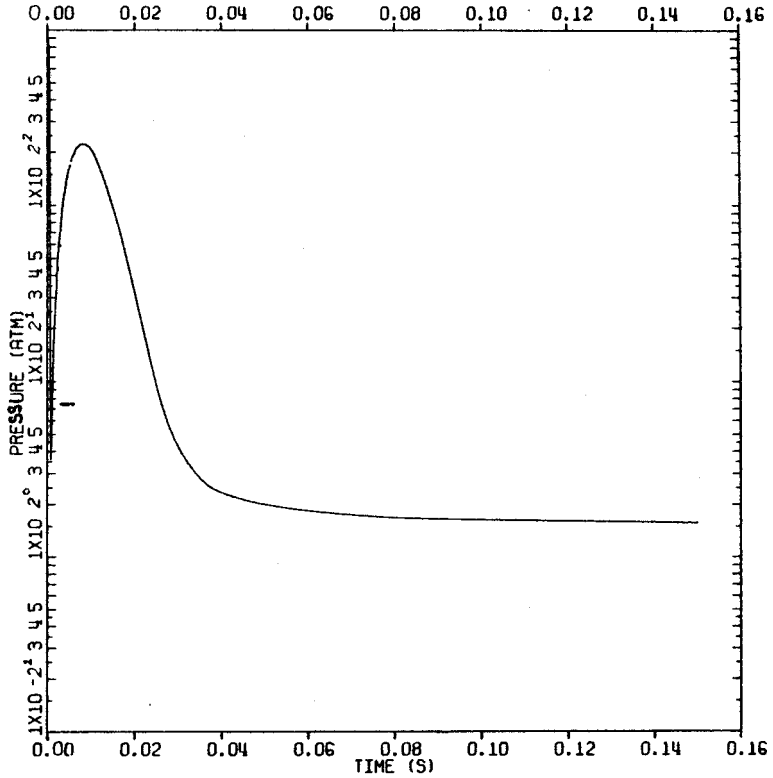

Figure 5.7 Pressure history for Case BURN-5H, which utilized nominal BURN parameter values and 9.6 g of fuel.

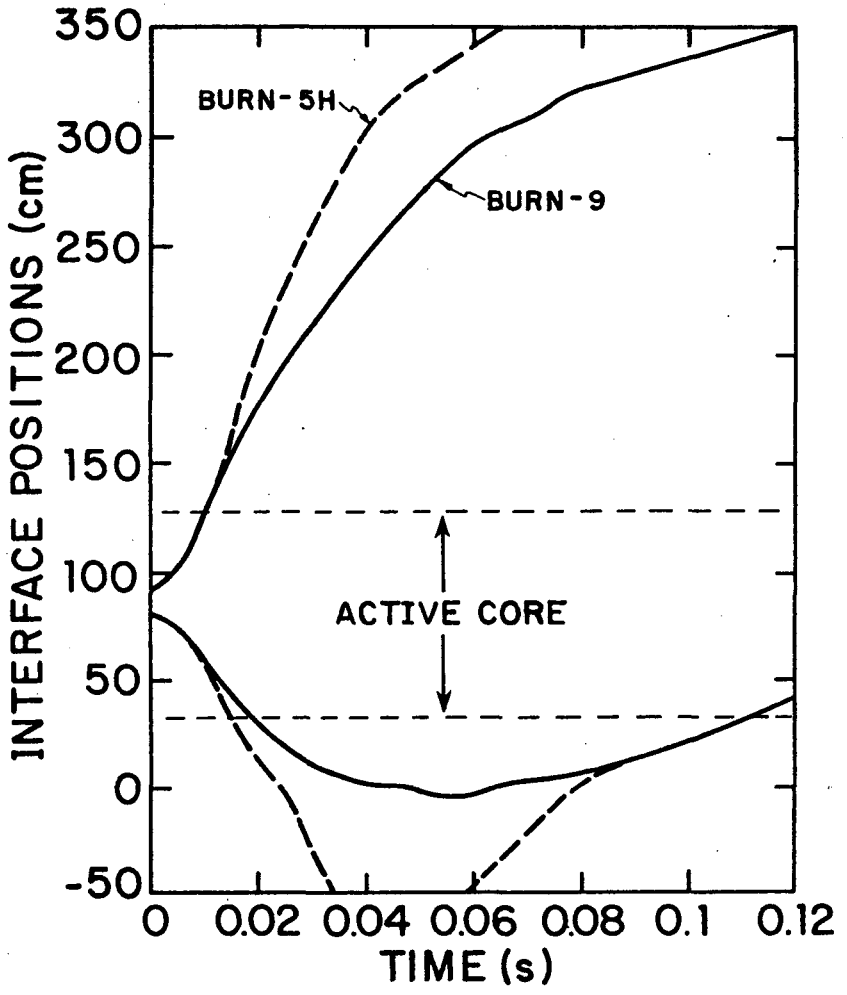

Figure 5.8 Effect on voiding history of tripling sodium-to-cladding heat transfer coefficient (Case BURN-9) above nominal value (Case BURN-5H).

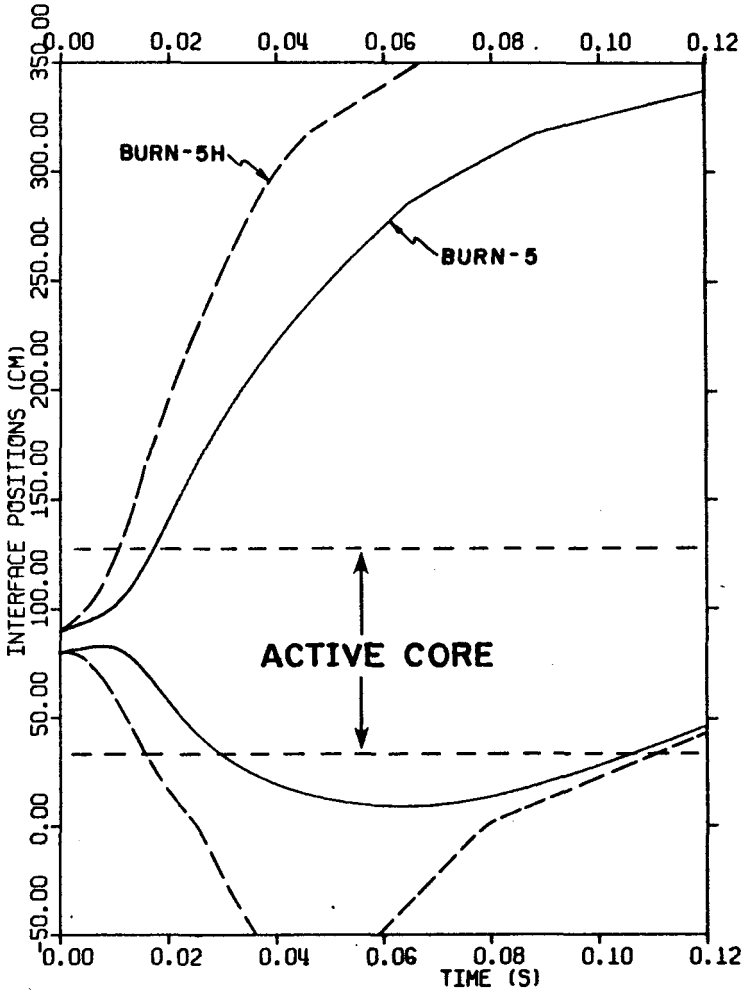

Figure 5.9 Reduction in voiding as a result of increasing fuel particle size from 200 microns (Case BURN-5H) to 632 microns (Case BURN-5).

BURN-9 (see Figure 5.8), with the original FCI zone region not yet reached by the returning lower sodium slug even at 150 msec after FCI initiation.

No cases were run which looked directly at separate variations in fuel mass and cladding temperature on the BURN-5H nominal case, but these effects are clearly illustrated with comparisons of other BURN series runs. Figure 5.10 compares voiding histories for BURN-5 and BURN-6. Referring back to the previous paragraph, note that BURN-5 differed from BURN-5H only in particle diameter. BURN-6 differed from BURN-5 only in the initial cladding temperature. For BURN-6 this was 1200 K rather than the nominal 1100 K. The increase in extent of voiding at long times (> 50 msec) is obvious although not order-of-magnitude. (The results are consistent with Figure 5.5 which showed the effects of cladding temperature variations in BOL cases.) It is important to note that lower interface positions for BURN-6 are further down in the core at very long times (> 95 msec) than for the very energetic BURN-5H (see Figure 5.6). This is again the result of the higher two-phase sodium temperatures at the long times when sodium-to-cladding heat transfer completely dominates.

The effect of failure non-coherence (which is primarily the effect of reducing available fuel masses) is illustrated in Figure 5.11. Here BURN-6 voiding is compared with BURN-8, for which the only change from BURN-6 was a halving of fuel and sodium masses. BURN-8 considered 4.8 g of fuel interacting with .8 g of sodium. The reduction in voiding for BURN-8 is as expected; however, the voiding is still impressive, with the lower slug requiring approximately 140 msec after FCI initiation to return to the bottom of the initial FCI zone. Remember that BURN-8 assumed large (632 micron) particle sizes as well as the smaller fuel and sodium masses which mock up non-coherence.

In the same vein as comments at the end of Section 5.1, we certainly admit to being able to combine selected values of the key parameters in ways to give much more or much less voiding for burned pins than for the nominal case, BURN-5H. However, it seems clear from the results illustrated in Figure 5.11 that the required mass of ejected and fragmented molten

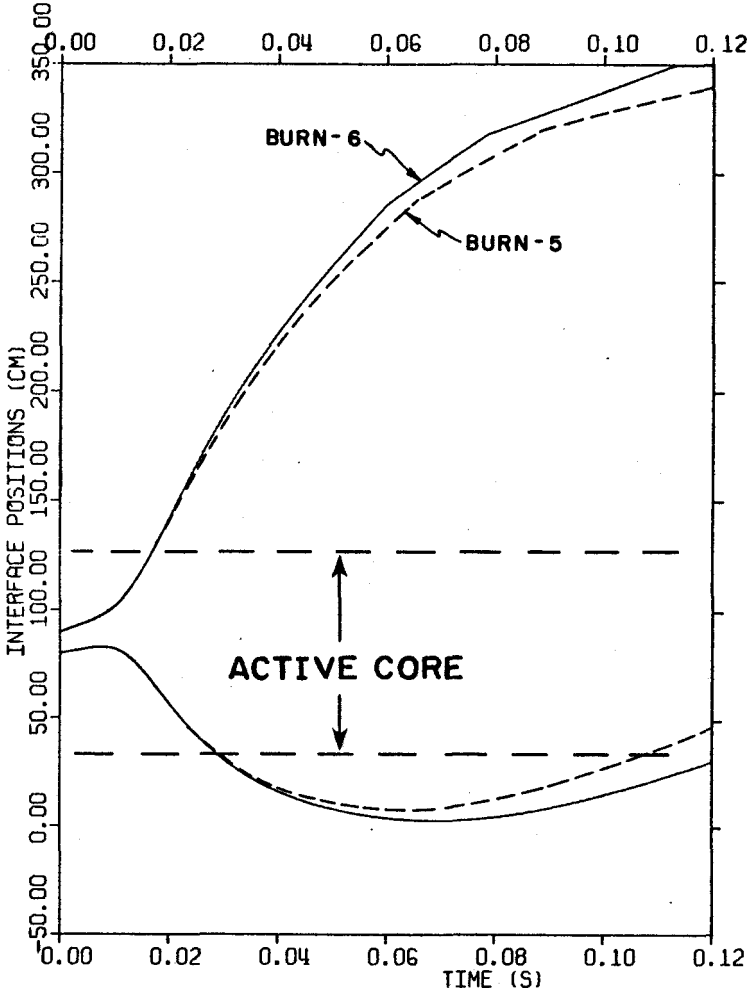

Figure 5.10 Effect of increased T_{ci} on voiding histories; for BURN-5, T_{ci} = 1100 K, for BURN-6, T_{ci} = 1200 K.

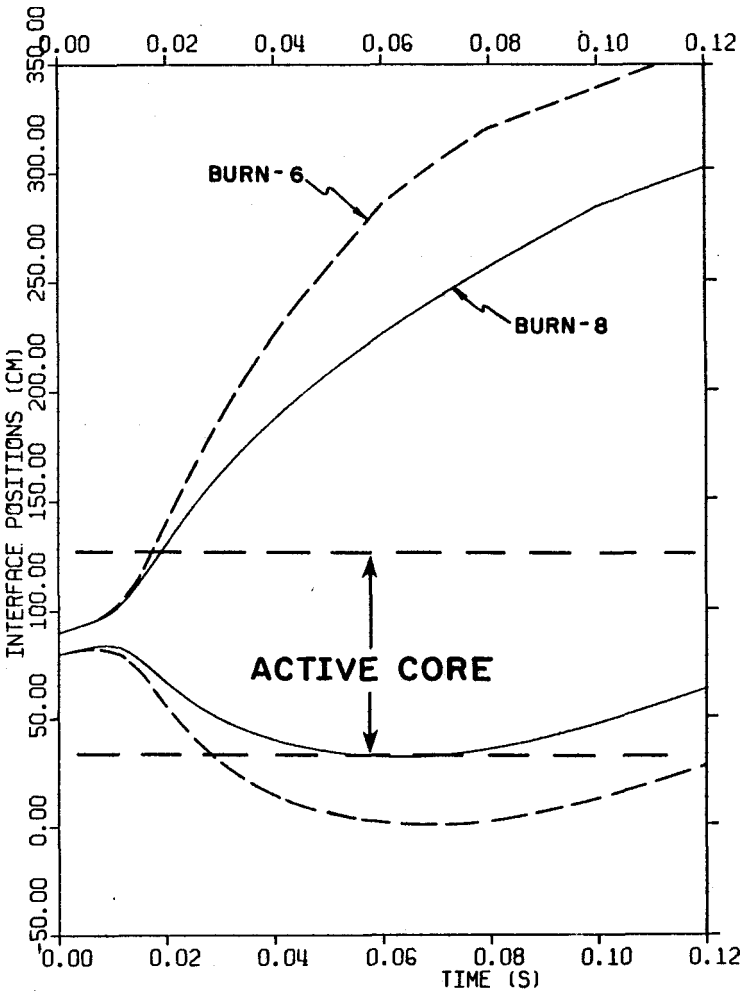

Figure 5.11 Reduction in voiding resulting from consideration of failure non-coherence (Case BURN-8) relative to coherent failure (Case BURN-6).

fuel per failed pin can be argued to be less than 5.0 g for coherent failure of 50% or more of the pins in a single subassembly. This mass is the order of 10% of the molten fuel mass available at pin failure.

5.3 General Conclusions

The parametric studies have led us to conclude that extensive subassembly voiding can be achieved following pin failure with small masses of molten fuel involved per pin (< 5.0 g). In order to have vigorous voiding during the early period when fuel-to-sodium heat transfer clearly dominates over sodium-to-cladding particle, diameters in the range of 200 microns must be assumed. For extensive long-term voiding (i.e. when sodium-to-cladding heat transfer dominates) the key parameter in our work was seen to be initial cladding temperature. This effect is not properly modeled either in PLUTO I or the current version of UVAFCI because axial distributions in initial cladding temperatures are not considered.

The effect of the magnitude of the sodium-to-cladding heat transfer coefficient, h, is important, but can act in different ways. The maximum observed downward voiding is decreased significantly as h increases; however, for long-term voiding in cases with high initial cladding temperatures, larger h values help to maintain voiding as the cladding acts to pump up the FCI zone.

REFERENCES
(Section 5)

1. Clinch River Breeder Reactor Project Preliminary Safety Analysis Report, Appendix F, pp. 6.2-7.

2. C. A. Erdman, M. B. Johnson, and A. B. Reynolds, Quarterly Progress Report for Oct. 1. 1975-Dec. 31, 1975, NRC Contract No. AT(49-24)-0158, University of Virginia.

3. H. U. Wider, "An Improved Analysis of Fuel Motion During an Overpower Excursion," Ph.D. Dissertation, Northwestern University (June 1974).

4. P. M. Haas, "Improved Modeling of the Fuel-Coolant Interaction in the Hypothetical Core-Disruptive Accident for the Liquid-Metal Fast Breeder Reactor," Ph.D. Dissertation, Nuclear Engineering Department, University of Virginia, pp. 136-139 (1974).

5. D. R. Armstrong, F. J. Testa, and D. Raridon, Jr., "Molten UO_2-Sodium Dropping Experiments," TANS, 13, 660 (November 1970).

6. PLENUM FISSION GAS RELEASE

Our original interest in plenum fission gas release paralleled that of our FCI interest, i.e. potential production of long-term, extensive voiding during a classical TOP such that fuel ejected from the pin might not be easily fragmented and removed from the core region. This interest was stimulated by the E7[1] test in TREAT.

We have also become interested in plenum gas release effects in the Loss-of-Flow (LOF) and Loss-Of-Flow-Driven TOP (LOF-D-TOP). In both of these latter situations, the gas release effects could be more important than in the classical TOP. In the high-power LOF channels, gas release may strongly affect or effect both cladding and fuel motion. In the LOF-D-TOP channels, the potential voiding due to plenum gas release is much more extensive than for the classical TOP because of the lower driving pump heads applicable to LOF-D-TOP.

Work done on the study of plenum gas release during CDA's has improved our understanding both of the heat transfer processes and of the modeling requirements involved. A simulation code for gas release called GASFLO has been written and used for initial simulation studies. We expect GASFLO to provide further guidance on requirements for plenum gas release modeling, and on the possible effects of that release on the overall accident scenario.

6.1 Comparison with Published Results

To test our computational techniques and develop a basis for further studies, we have attempted to reproduce the voiding history presented in Reference 2, using the isothermal flow model described in that report. The ANL model for coolant slug motion assumes one-channel flow through the outlet module, which overestimates the inertial constraint to upward voiding of a single subassembly; the use of this constraint model and the use of a very high initial plenum gas pressure both contribute to pronounced downward motion of the lower coolant slug. Inclusion of both these factors in GASFLO, however, did not give us downward voiding rates equivalent to those in the ANL report. The complexity associated

with modeling flow in the lower subassembly structure leads us to suspect that the difference lay in the computation of the pressure retarding downward voiding. Therefore a GASFLO run was made with 0.1 MPa (1.01 atm) less retarding pressure than our best estimate for the CRBR design. This produced a voiding history similar to that of the ANL report.

6.2 CRBR Calculations

As indicated in Section 6.1, we were able to generally reproduce the results of Reference 2. The plenum pressures used in the ANL studies (1700 psia or about 12 MPa) correspond to 2σ confidence upper limits at EOEC as presented in the PSAR. Our own estimates for EOEC were considerably less than this; moreover, we have an immediate interest in the early CRBR cores before the true equilibrium cycle has been obtained. Therefore, we also looked at voiding histories for gas plenum pressures of 7 MPa (~ 1000 psia).

Figure 6.1 shows voiding histories for coherent failure of all the pins in a single subassembly during a classical TOP for the two different initial plenum pressures given above. The failure was assumed to occur at the top of the active core. Gas flow parameters (e.g. blanket-cladding gap size) were the same as those in Reference 2. Our own CRBR hydraulics model was utilized. This gives slightly weaker downward voiding in the 12 MPa case than the voiding predictions of Reference 2.

For the case with a 7 MPa initial plenum pressure, the voiding effectively does not extend down into the active core. Conversely, for the 12 MPa case, the active core sees significant voiding and is not completely covered again until more than 250 msec after pin failure. This 12 MPa case could be significant in terms of failing pins and ejecting molten fuel into a voided region. However, for the first core, the 7 MPa case represents an upper limit, and if non-coherence in failure is considered in the 12 MPa case, the voiding history will be very similar to (in fact probably weaker than) the 7 MPa case.

Based on the results of Figure 6.1 and the comments made above, the plenum gas voiding would not seem to be as important in the classical

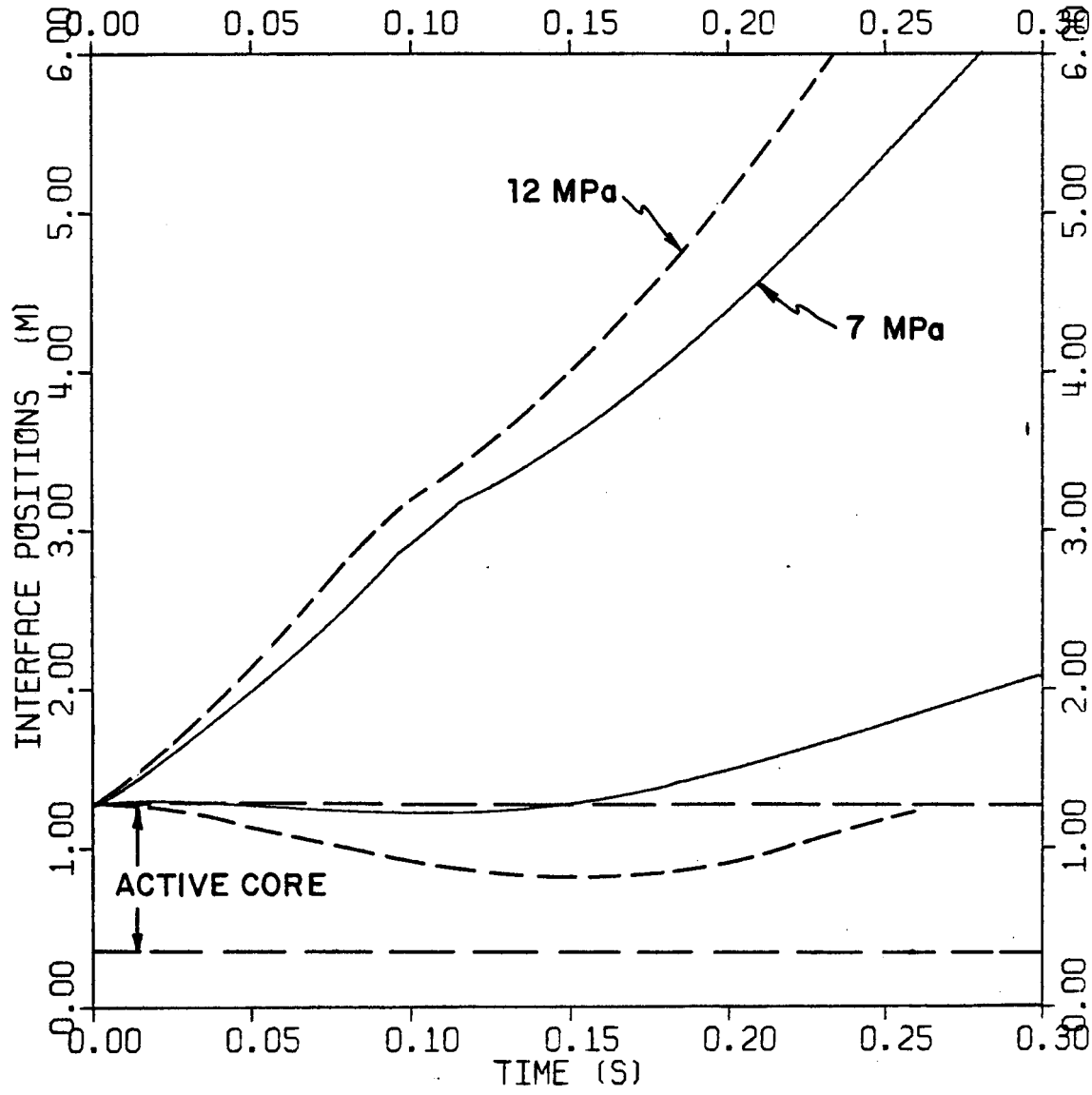

Figure 6.1 Voiding histories for plenum gas release; the effect of variation in initial plenum pressure (7 vs. 12 MPa) is illustrated.

TOP as we had originally anticipated - at least for the case where the gas release at the core-upper-blanket interface corresponds to the initial failure.

6.3 Heat Transfer Processes

The analysis of Reference 2 assumes that the fission gas behaves isothermally throughout the transient. It was not clear to us that this is the case in the plenum, in the gap, or in the coolant channel. Early calculations showed that if heat transfer from the cladding were ignored, the gas remaining in the plenum would drop significantly in temperature as it depressurized. Also, we began looking at possible alternate behavior[3] for the gas flowing in the annulus. It became necessary to make at least some rough estimates on heat transfer rates at each point in the gas flow in order to determine whether or not the flow was even close to isothermal.

6.3.1 Gas Remaining in Plenum

The temperature of gas remaining in the plenum during the expulsion process would indeed drop the order of 100 K or more in temperature if no heat transfer from the cladding to gas were considered. For simple estimates of the times for heat transfer via conduction from the cladding walls to stagnant xenon gas within the plenum we looked at Fourier numbers of unity, i.e. $\frac{\alpha t}{R^2} = 1.0$, where α is the thermal diffusivity of the gas, R is the I.D. of the plenum cladding, and t is time. The time constant of interest for this process under initial plenum conditions of 7 MPa pressure (~ 1000 psia) and 900 K temperature is about 5 seconds. Since the rapid gas expulsion process of interest is over in the order of 1.0 sec or less, conduction heat transfer from the cladding could be ignored. However, since the gas is not stagnant, a convective mode must be considered.

For this mode, the time constant of interest would be $\left(\frac{R^2}{\alpha}\right)\left(\frac{k}{2hR}\right) = \left(\frac{R^2}{\alpha}\right)\left(\frac{1}{Nu}\right)$ where Nu is the Nusselt number, k is the gas thermal conductivity, and h is the convective heat transfer coefficient. The value of Nu will vary along the plenum during gas expulsion as gas flows down to the

blanket. Based on calculations using a developmental code which was a precursor of GASFLO, values of Nu at the bottom of the plenum can be the order of 60 with h = .02 $W/cm^2 \cdot K$. This reduces the time constant for heat transfer at that point to less than 100 milliseconds, and would seem to make heat transfer important. However, along the plenum, Nu will vary from 60 at the bottom down to essentially zero at the upper end of the plenum. A detailed calculation will be necessary if the 100 K variation in plenum gas temperature predicted in preliminary calculations is found to be important in terms of explusion rates.

6.3.2 Gas Flowing in the Blanket-Cladding Gap

In the annular region between the upper blanket and surrounding cladding, values of h will be sufficiently high to insure that the gas quickly achieves a local temperature based on some average of the blanket and cladding temperatures. Values for Nu and h would be the order of 35 and 3.5 $W/cm^2 \cdot K$ respectively in the gap.

Apparently then the gas temperature will be controlled by the blanket and cladding temperatures; this, however, will not be an isothermal situation, since the blanket and cladding temperatures vary axially. Moreover, at the rupture site where the gas enters the coolant channel, a rapid deceleration in gas velocity will occur with a resulting rise in temperature.

6.3.3 Gas Flow in the Coolant Channel

Rapid variations in volume, flow rates, and densities complicate the analysis of gas flow in the coolant channel. Similarities in equivalent diameter, flow area, and mass transfer to those of the fission gas plenum on a per pin basis are offset by the lower gas density and possible density gradients in the gas. If no mechanistic treatment is developed for the channel flow, the extremes of thermal behavior (i.e. adiabatic and isothermal flow) will be modeled to scope the possible effects of heat transfer in this region.

6.4 Gas Release Calculational Sensitivity

The sensitivity of gas release histories to the assumptions made in

modeling gas flow in the fission gas plenum, gap, and coolant channel, is being tested by examining simulations of the extremes of heat transfer behavior in each region: adiabatic flow (isolation of the gas from the clad/blanket) and isothermal (immediate equilibration of gas and clad). The degree to which variables of interest are sensitive to our assumptions will determine the necessary complexity of gas release models for accurate accident analysis.

Such a sensitivity study has already been performed for the annular blanket-clad gap. We have compared isothermal and Fanno (adiabatic) flow in the annular gap for the same driving pressures, and have found little or no difference in predicted mass flow rates or in predicted pressure drops. The two models predict considerably different gas temperatures on delivery to the coolant channel, and it remains to be determined if the accident history will be significantly affected by this difference; the results of the study, however, indicate that the simple isothermal model is probably an adequate model of the gap flow.

REFERENCES
(Section 6)

1. A. B. Rothman et al., "Review of TREAT Experiments in Support of Transient Overpower (TOP) Analysis for Fast Reactor Safety," Proc. ANS Fast Reactor Safety Conference, Beverly Hills, Calif., CONF-740401, pp. 205-219 (April 1974).

2. T. C. Chawla et al., "The Rate of Coolant Recovery Following Rapid Release of Fission Gas from a Postulated Multiple Pin Failure in an LMFBR Assembly," TANS, 20, 315 (June 1975).

3. C. A. Erdman, M. B. Johnson, and A. B. Reynolds, Quarterly Progress Report for Jan. 1, 1976-March 31, 1976, NRC Contract No. AT(40-24)-0158, University of Virginia.

7. EARLY FUEL BEHAVIOR IN THE SODIUM CHANNEL IN A TRANSIENT OVERPOWER ACCIDENT

7.1 Objectives of Current Work

The purpose of the work described here was to understand the phenomena involved in the early motion of fuel into the sodium following fuel pin failure in a TOP accident. Such an understanding is necessary in order to assess the validity or adequacy of models currently being used for analysis of these phenomena. Controlling processes in early fuel motion and weaknesses and uncertainties in the current modeling of these processes should be identified.

7.2 Processes in Early Fuel Motion

When a fuel pin ruptures in a TOP accident, fuel may be expelled from the pin by fuel vapor pressures or by gases (resulting from fission or manufacturing) which may have been in an initial central void or are released from the hot fuel. We are mostly concerned here with burned pins, for which fission gas is the primary fuel ejection force. The first fuel to emerge may still be solid. This will be followed by molten fuel which may be mixed with fission gas.

As molten fuel encounters sodium, several competing processes can occur. The fuel will compress the sodium in order to create volume to accommodate the emerging fuel. The sodium must be analyzed as a compressible constraint for the first one or two milliseconds. (After several milliseconds the compressed sodium starts to act in the same manner as an incompressible slug.) The fuel will tend to fill the space in the sodium channel between the adjacent fuel pins at the level of the rupture. Simultaneously the flowing sodium tends to drag the fuel along with it, exerting shear forces along the vertical fuel surfaces and inertial forces (from the dynamic pressure of the sodium) against horizontal fuel surfaces. The geometry for a slit rupture is illustrated in Figure 7.1. At position (a) in the motion, the principal forces on the fuel may be shear forces. At position (c), however, the principal forces are the inertial forces which result from the dynamic pressure of the flowing sodium.

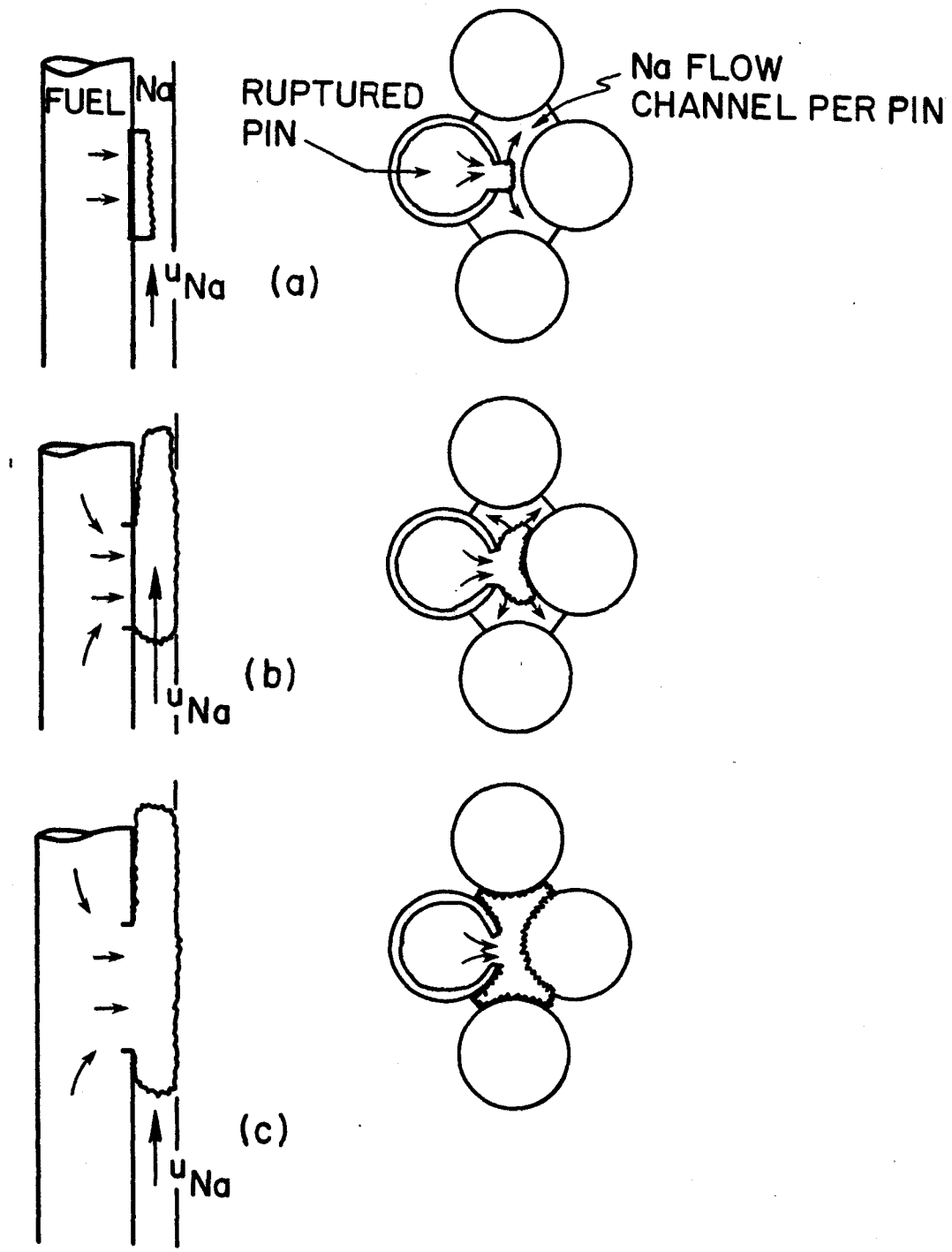

Figure 7.1 Early fuel motion from a slit rupture.

Up to the time when significant solidification of the fuel takes place, the flowing sodium will act to fragment the liquid fuel. This hydrodynamic fragmentation can occur if the Weber number exceeds a critical value, where the Weber number is the ratio of an inertial or shear force (which tends to fragment the fuel) to a surface tension force (which opposes breakup). Even if the critical Weber number is exceeded, however, there may be insufficient time for hydrodynamic fragmentation to occur prior to solidification of the fuel.

During the early motion of the fuel the sodium also rapidly cools the surface of the fuel and tries to solidify the outer part of the fuel. Cronenberg[1] has shown that this solidification rate is controlled by the rate of conduction, as opposed to the rate of nucleation of solid fuel. Cronenberg, Chawla, and Fauske[2] and others[3] have also shown that thermal stresses in the resulting crust of solid fuel are likely sufficient to fragment this crust. In this report we label this process thermal fragmentation, as opposed to hydrodynamic fragmentation referred to in the previous paragraph.

If the fuel fragments, sufficient surface area can be generated to produce a local fuel-coolant interaction (FCI). This FCI is of the type often referred to as "vigorous boiling" because the interface surface termperature of the sodium is below the spontaneous nucleation temperature of the sodium. Hence what Fauske[4] calls a true "vapor explosion" or even "continuous explosive boiling" does not take place even on this local level. This vigorous-boiling type of FCI is the type modeled by the FCI module of SAS and by PLUTO.

7.3 Analysis of Processes During Early Fuel Motion

In order to meet the objectives of this study, three analyses were made or are under way. First, a PLUTO calculation was made which involved only hydrodynamic processes; heat transfer from fuel to sodium was eliminated, thereby excluding any FCI. These results were compared with hand calculations of some of the principal flow processes. Second, calculation of hydrodynamic fragmentation of liquid fuel by flowing sodium were initiated. Third, rates of solidification and buildup of

thermal stresses have been estimated in order to compare the potential for thermal fragmentation with the potential for hydrodynamic fragmentation.

7.3.1 PLUTO Run to Examine Hydrodynamics of Early Fuel Motion

The PLUTO code models the flow of fuel inside the fuel pin toward the rupture, the compressible response of the sodium as the fuel emerges, and the compressible response of the sodium during a resulting local FCI. Resistance to fuel flow at the rupture is assumed to be negligible relative to the sodium constraint and to resistance to fuel motion within the pin. (This assumption may be difficult to defend for many failure conditions, but currently it is generally accepted.) It is further assumed that all of the fuel fragments into particles of a user-selected size as the fuel emerges from the rupture. The length of the rupture must be the length of the axial node where the rupture is assumed to occur . The width of the rupture is irrelevant since the amount of fuel which emerges is completely controlled by the change in sodium volume in the sodium channel resulting from sodium motion.

A PLUTO run which modeled failure of a burned pin in a 50¢/sec transient was made in order to examine hydrodynamic processes during the early expulsion of fuel. Heat transfer was effectively eliminated by decreasing the thermal conductivity of the fuel by a factor of 10^5 and by using a fuel particle diameter of 5 mm. Drag forces by the sodium on the emerging fuel were low relative to gravity since the particle size was so large.

In this PLUTO calculation, liquid fuel emerged from the pin rupture, remained effectively unfragmented, and was dragged only a short distance during the 20 milliseconds duration of the calculation. The node length over which the rupture was assumed to occur was 59.2 mm. The pressures in the pin and channel adjusted as the fuel compressed the sodium in the channel while fuel flowed inside the pin toward the break.

Prior to the rupture, the pressure in the fuel pin was 16.2 MPa (162 bars). The pressure in the sodium at the rupture location was 0.6 MPa. Immediately after the rupture, communication between the fuel

and the sodium caused the pressure in the pin to drop to 11.5 MPa while the pressure in the sodium in the node adjacent to the rupture instantaneously rose to virtually the same value, or 11.2 MPa. This pressure then compressed the sodium, making space for fuel to emerge.

The pressure at the rupture very rapidly dropped to 5 MPa (in 0.1 msec) in both the fuel and the sodium, and slowly decreased thereafter to 3 MPa at 2 ms and 1 MPa from 5 ms to 20 ms. Pressures at the rupture, together with the mass of fuel ejected from the pin, are listed in Table 7.1 for various times after failure.

Table 7.1

Pressure at Rupture Location and Fuel Ejected from One Pin as Calculated by PLUTO, with No Heat Transfer to the Sodium

	Pressures at Rupture		
Time (ms)	Fuel (MPa)	Sodium (MPa)	Fuel Ejected (g)
0	16.2	0.6	0
0+	11.5	11.2	0.03
0.1	5.2	5.2	0.14
1	5.0	4.7	0.76
2	3.1	3.0	1.57
5	0.9	0.8	5.12
10	1.0	1.0	9.56
20	1.2	0.7	15.2

In studying potential heat transfer prior to thermal fragmentation and hydrodynamic fragmentation processes, it is of interest to examine the geometry of the fuel in the channel. In particular, it is of interest to know what fraction of the sodium flow area in the channel is occupied by the fuel. The PLUTO run provides us with that information. At 2 ms, 1.51 of the 1.56 g of fuel in the channel is still in the node containing the rupture. For the 59.2 mm long node, a sodium flow area per fuel pin of 20 mm^2, and a fuel density of 8.1 g/cm^3, the calculated fraction of the channel occupied by fuel at 2 ms was 0.16. At 20 ms, the 15.2 g of fuel was distributed fairly evenly over four nodes. Hence at this time

the fuel occupied about 40% of the flow area. For smaller size particles than the assumed 5 mm diameter, fuel would be dragged somewhat faster from the rupture so that it would occupy smaller fractions of the flow area.

7.3.2 Approximate Hydrodynamic Model for Early Fuel Motion

As indicated above, after failure of the cladding, fuel moves through the rupture and compresses the sodium in the channel. Fuel flows internally in the pin to the failure location. PLUTO accounts for the compression of the sodium and ignores any resistance at the cladding rupture.

In order to make sure that we understood and agreed with the PLUTO results, a simple calculation was made to reproduce the PLUTO prediction of fuel expulsion into the channel during the first millisecond as follows.

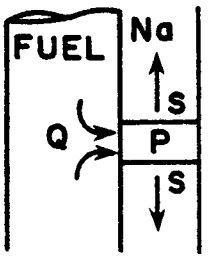

Figure 7.2 Geometry for early fuel motion and compression of the sodium.

The volume change generated by a pressure in one-dimensional geometry is given by the compressible constraint equation:

$$P - P_o = \frac{\rho_{Na} c}{2S} \cdot \frac{dV}{dt} \qquad (1)$$

where V = volume displaced

c = velocity of sound in sodium (2.7×10^3 m/s)

ρ_{Na} = sodium density (0.78 g/cm^3)

S = flow area (20 mm^2)

P = pressure in the expanding zone

P_o = initial pressure in the zone.

Twice the area S is utilized since the sodium is compressed in both directions.

The volumetric flow rate, Q, of fuel through the rupture is equal to $\frac{dV}{dt}$. The mass of fuel which enters the channel in time t is $\int_o^t \rho_f Q dt'$ where ρ_f is the fuel density (8.1 g/cm^3).

In the PLUTO run described in Section 7.3.1, the pressure was ~ 5 MPa from 0.1 ms to 1 ms. Assuming a constant P of 5 MPa (and neglecting P_o) gives for the mass of fuel ejected in 1 ms

$$m_f = \rho_f Q t = \frac{2PS\rho_f t}{\rho_{Na} c}$$

$$= 0.77 \text{ g}$$

which is in approximate agreement with the PLUTO result listed in Table 7.1. After about two milliseconds, the PLUTO results diverge significantly from this simple model.

In the PLUTO calculation, the pressure in the fuel and the channel at the node where the rupture occurs immediately equalizes because resistance to flow at the break is neglected. If the rupture were not a long rip but was instead a hole or a break of small height, this resistance might become appreciable.

If the break is considered as an orifice, with ejection friction coefficient c_d, the pressure loss between fuel at pressure P_f and the sodium channel at pressure P can be written as

$$P_f - P = \frac{1}{c_d^2} \frac{\rho_f u_o^2}{2}$$

where u_o is the velocity at the orifice. In terms of the volumetric flow rate of fuel, $Q = u_o A_o$, where A_o is the orifice area,

$$P_f - P = \frac{1}{c_d^2 A_o^2} \frac{\rho_f Q^2}{2}.$$

Combining this with Equation (1), ignoring P_o, and recognizing that $Q = \frac{dV}{dT}$, gives a quadratic equation for Q:

$$Q^2 + \frac{\rho_{Na} c_d^2 A_o^2 c}{\rho_f S} Q - \frac{2 c_d^2 A_o^2 P_f}{\rho_f} = 0. \qquad (2)$$

When the flow resistance at the rupture is low, the Q^2 term is far smaller than the other two, P_f becomes equal to P, and Equation (2) reduces to Equation (1).

7.3.3 Hydrodynamic Fragmentation

If the molten fuel which emerges from the rupture fills most of the sodium channel as in Figure 7.1 (c), the inertial force of the sodium (i.e. the dynamic pressure) will tend to fragment the fuel. If the fuel emerges from a long slit in the cladding and fills only part of the sodium channel as in Figure 7.1 (a), the fuel will appear as a long thin slab with sodium flowing along the surfaces of the slab. In this case the shear force or drag exerted by the sodium will tend to fragment the fuel. In either case surface tension will be the force which resists fragmentation.

When an inertial force tends to fragment liquid fuel filling the channel, the appropriate Weber number for evaluating fragmentation is

$$We = \frac{\rho_{Na} u^2_{Na} D}{\sigma_f}$$

which is proportional to the inertial force $\frac{\rho_{Na} u^2_{Na}}{2} \cdot \frac{\pi}{4} D^2$ divided by the surface tension force, $\pi \sigma_f D$. The appropriate D here is defined by Figure 7.3.

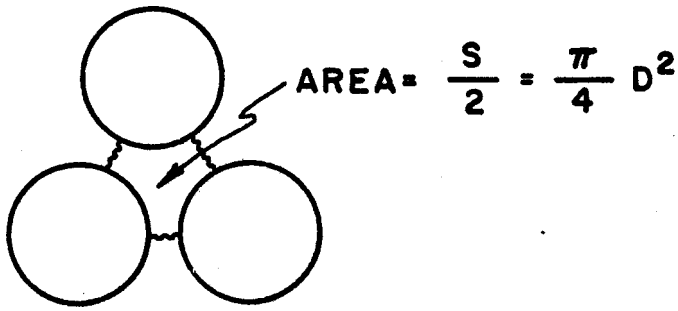

Figure 7.3 Geometry for inertial force in Weber Number (S is defined as the sodium flow area per pin, half of which is shown here).

Liquids are fragmented by inertial forces when a critical Weber number, We_c, is reached. The value of We_c is of the order of 10 to 20 (for example, Reference 5).

When shear forces are responsible for breakup, the shear force exerted by the sodium on the fuel slab of surface A is $A\mu_{Na}\frac{du}{dy})_{Surface}$, where $\frac{du}{dy}$ is the velocity gradient in the sodium perpendicular to the fuel slab. The geometry is shown in Figure 7.4.

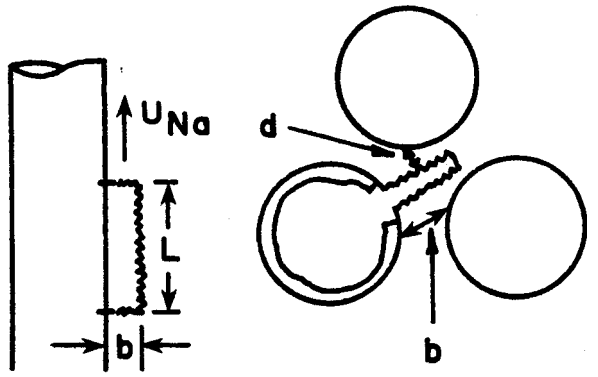

Figure 7.4 Geometry for shear forces on fuel slab.

The gradient $\frac{du}{dy}$ would be represented in a Weber number by the sodium velocity u_{Na} divided by the small distance, d, in the sodium flow channel between the fuel and an adjacent fuel pin. The area A is Lb. The surface tension force resisting fragmentation would be σb. The appropriate Weber number for fragmentation by the shear force would be:

$$We = \frac{\mu_{Na} u_{Na} L}{\sigma d} .$$

Information on breakup directly by shear forces was not found in the literature; however, values of this We anticipated for CRBR conditions would seem too small for fragmentation by shear forces.

For $\mu_{Na} = 1.79 \times 10^{-4}$ Pa•s, $u_{Na} = 6$ m/s, $\sigma_f = .5$ N/m, L = 50 mm, and d = 2.5 mm, the appropriate We is 0.043. By comparison, Weber numbers for the inertial forces involved when fuel fills the entire sodium channel can be calculated. For $\frac{S}{2} = 10\ mm^2 = \frac{\pi}{4} D^2$, $D = 3.6 \times 10^{-3}$ m, again assume $u_{Na} = 6$ m/s, and $\sigma_f = 0.5$ N/m. Then for $\rho_{Na} = 780\ kg/m^3$, we have We = 200. This high value of We indicates that the fuel would be

fragmented by hydrodynamic forces if it remains molten long enough or if the frozen surface is sufficiently thin and weak.

There appears to be a competition between thermal and hydrodynamic fragmentation. It is therefore of interest to examine how long it might take for hydrodynamic fragmentation to occur and to compare this time with the time required for freezing and thermal fragmentation of the fuel.

The time required for hydrodynamic fragmentation due to interfacial instability has been correlated by means of another dimensionless group[6], the Bond number;

$$Bo = \frac{\rho_f g D^2}{\sigma_f}$$

where g is the acceleration of the liquid globule exerted by the fluid flowing past it, and ρ_f and σ_f are properties of the liquid globule For $Bo > 40$, surface instabilities result from gas flowing over liquid globules. For $Bo > 10^4$, these instabilities lead to fragmentation in a time, t, correlated as:

$$\frac{\rho_{Na}}{\rho_f} \frac{u_{Na} t}{D} \sim 46\ Bo^{-1/4} \qquad (3)$$

In Reference 6, Bo and a dimensionless time, t*, are defined in terms of radius instead of diameter. Hence a coefficient of 65 appears in Reference 6 instead of 46.

For $40 < Bo < 10^4$, fragmentation will tend to occur slowly from a steady distortion by inertial forces instead of from surface instabilities.

In order to estimate Bo under the flow conditions described above for which We = 200, it is necessary, to evaluate g. To do this, let us assume that the liquid globule is a sphere of diameter D = 3.6 mm. The drag force exerted on a sphere of fuel by sodium flowing around it is related through a drag coefficient, C_D,

$$F = \frac{C_D \rho_{Na} u_{Na}^2}{2} \frac{\pi}{4} D^2$$

This force accelerates the sphere according to the relation

$$F = M_{sphere} g = \frac{\pi \rho_f D^3}{6} g$$

Hence,

$$g = C_D \frac{\rho_{Na}}{\rho_f} \frac{3}{4} \frac{u_{Na}^2}{D}$$

The drag coefficient is related to the Reynolds number. For the large Re numbers associated with sodium flow through the channel and the spherical diameter of 3.6 mm, $C_D \sim 3$. This gives a value of g of the order of 2200 m/s^2. The Bond number, therefore, is of the order of Bo ~ 500.

This value is below the range of data in Reference 6 and is in the range where hydrodynamic fragmentation may occur from steady distortion rather than surface instabilities. However, if the fragmentation did occur from surface instabilities according to Equation (3), then the time required for hydrodynamic fragmentation would be ~ 60 milliseconds.

7.3.4 Thermal Fragmentation

The fragmentation of molten fuel following contact with liquid sodium has been observed experimentally for both in- and out-of pile tests. The one mechanism that can be consistently argued to operate in all of these tests is that of thermal fragmentation associated with solidification of the fuel. Cronenberg and Grolmes[1] have provided a review of fragmentation theories and have presented arguments for the thermal stresses developed followed UO_2-Na contact as being the "most immediate cause for fragmentation." The work of Knapp[3] generally supported the conclusions of Cronenberg and Grolmes although he differed somewhat in details of calculational results and requirements for fragmentation.

The work of Cronenberg et al. of Reference 2 predicts peak total stress values (a combination of thermal and pressurization stresses) to occur at contact times consistent with experimentally observed delay times for fragmentation. The stress calculations are summarized in Reference 1. For a spherical UO_2 particle initially at its melting

point and sodium at 200° C, the total surface tangential stress peaks at about 50 msec after contact, while referenced experiments were said to give delay times of 30 to 80 msec.

The molten UO_2 droplets considered in References 2 and 3 were large (0.72 cm in diameter) compared to possible characteristic dimensions of molten UO_2 within prototypic coolant channels. As pointed out in an earlier section, dimensions of 0.36 cm would represent an upper limit, while for completely spherical UO_2 droplets, diameters more of the order of 0.25 cm would be more appropriate. The major effect of size scaling in stress calculations such as those of Reference 2 is to give a different time scale for the solidification and stressing processes.

If the controlling resistance to heat flow is in the UO_2 rather than at the UO_2-Na interface, the parameter which will describe time scaling for various droplet sizes is, of course, the Fourier modulus, $\alpha t/R^2$, where α is the UO_2 thermal diffusivity, R is the particle radius, and t is the time since contact of the UO_2 and sodium. This parameter provides us with a convenient means of estimating fragmentation times for smaller droplets from the results of Reference 2 plus supporting experimental results. A reduction of droplet radius by a factor of two (i.e. from 0.36 cm to 0.18 cm) changes time scales by a factor of four and suggests times for fragmentation of the order of ten milliseconds. Considering droplets with a 0.12 cm radius brings the time scale down to 5 to 6 msec.

These short times estimated for thermal fragmentation indicate that thermal fragmentation would dominate hydrodynamic fragmentation, which we estimated earlier to have time scales of the order of 50 msec based on surface instabilities.

Reference 1 also suggests that the particle size distribution resulting from thermal fragmentation is a normal Gaussian distribution in the log of the particle size. This suggestion is based on an examination of available fragmentation experimental results. The most probable mass-mean particle size for the "fines" would be approximately 200 μm, consistent with values utilized in our parameter studies.

7.4 Application to Overall Voiding Analyses

From the arguments of this section, we reached two primary conclusions:

(1) For a large-area failure having no resistance to flow at the rupture site, 5 to 10 grams of molten fuel can be ejected from the pin and into the coolant channel during the first few milliseconds following pin failure.

(2) The molten fuel will probably be fragmented within 5 to 10 milliseconds after contacting liquid sodium. The fragmentation will probably result from solidification phenomena, although hydrodynamic fragmentation is possible over an extended period.

REFERENCES
(Section 7)

1. A. W. Cronenberg and H. K. Fauske, "UO_2 Solidification Phenomena Associated with Rapid Cooling in Liquid Sodium," J. Nucl. Mater., 52, 24-32 (1974).

2. A. W. Cronenberg, T. C. Chawla, and H. K. Fauske, "A Thermal Stress Mechanism for the Fragmentation of Molten UO_2 upon Contact with Sodium Coolant," Nucl. Eng. Des., 30, 434-443 (1974).

3. R. B. Knapp, "Thermal Stress Initiated Fracture as a Fragmentation Mechanism in the UO_2-Sodium Fuel-Coolant Interaction," Ph.D. Dissertation, Massachusetts Inst. of Tech. (May 1975).

4. H. K. Fauske, "Some Aspects of Liquid-Liquid Heat Transfer and Explosive Boiling," Proc. of ANS Fast Reactor Safety Conference, Beverly Hills, Calif., CONF-740401, pp. 992-1005 (April 1974.

5. J. O. Hinze, "Forced Deformations of Viscous Liquid Globules," Appl. Sci. Res., A1, 263-272 (1949).

6. P. G. Simpkins and E. L. Bales, "Water-Drop Response to Sudden Accelerations," J. Fluid Mech., 55, 629-639 (1972).

APPENDIX A*

SODIUM VOIDING IN LOSS-OF-FLOW-DRIVEN TRANSIENT OVERPOWER (LOF-D-TOP) ANALYSIS

A.1 Introduction

The possibility of rapid sodium voiding occurring in previously unvoided channels during advanced stages of the loss-of-flow (LOF) accident is one which is crucial to determination of the nature of the termination mode for the first prompt critical burst. DPM personnel have previously addressed the question of the role which a fuel-coolant interaction (FCI) might play in vigorous voiding[1]. Even when the positive reactivity effects of early fuel motion are ignored for an axially centered break, the positive reactivity effects due to sodium voiding may make a significant contribution to the overall ramp rate. Choice of FCI controlling parameters is a critical process in such calculations. The uncertainties involved may make such calculations susceptible to criticisms from both the applicant and intervenors.

In an investigation of alternate scenarios following pin failure, we have looked at the potential voiding due to cavity and froth gasses which are present in the low power channel pins at failure. This work was originally motivated by suggestions from J. Meyer of DPM that, for the long cladding rips and very weak cladding predicted in the LOF-D-TOP channels, a "squeeze-out" of sodium resulting from fuel gas pressurization might precede any significant FCI voiding and associated fuel motions. Modeling of these phenomena by simple hand calculation, the UVAFCI code, and SAS3A has indeed indicated that vigorous voiding is a possibility.

A third potential voiding mechanism for the LOF-D-TOP channels which has been given little attention to this point is the large scale release of gas from the fission-gas plenum. Cladding temperature histories calculated in SAS suggest that such releases would probably occur before failure times considered for FCI calculations in some DPM analyses. We

*This Appendix was submitted to NRC in July 1976 and has not been significantly revised since. Recent work has modified some of the concerns and conclusions expressed here.

feel that such releases could result in voiding rates comparable to those calculated from FCI or fuel gas considerations. Certainly this possibility should be examined.

We have mentioned in this introduction three potential mechanisms for vigorous voiding in LOF-D-TOP channels. The degree of operability of each of these mechanisms has not been clearly established. To discard these mechanisms without further investigation cannot be justified at this point. In the remainder of this appendix we will be concerned primarily with a more detailed discussion of the second of the three mechanisms: sodium squeeze-out induced by gas pressures within the fuel at pin failure.

A.2 Pressurization of Failure Region

The exact process involved here is not crucial to later arguments on voiding rates; this is fortunate, because the dynamics surrounding pin failure in the LOF-D-TOP channels are not well understood. Based on recommendations of other DPM consultants and personnel[2], we have been considering long cladding rips or "regions of severely weakened" cladding.

One could visualize the sodium pressurization resulting from phenomena such as fuel/gas attempting to enter the coolant channel through the cladding rip or from a ballooning of the extremely weak cladding. If the latter scenario is accepted, fuel motion can be neglected, although a positive reactivity effect could be expected from some net fuel motion toward the center of the pin. (This last comment and the next paragraph address one of the questions raised by ANL personnel and listed in Section A.6 of this appendix.)

If fuel is assumed to extrude out into the coolant channel, there would be some axial motion, but probably not within an order of magnitude of the artificial motion predicted by SAS/FCI. Thus, if one uses SAS/FCI to mock up this pressurization, it seems reasonable to ignore fuel reactivity effects. (Note that we ignore a small positive fuel motion effect for the ballooning scenario and a small negative effect for the extrusion scenario. This is reminiscent of Appendix D arguments in the original CRBR PSAR version.)

Whichever scenario is accepted, the driving force for sodium voiding is the fission gas in the molten fuel cavity at pin failure. This includes both central cavity gas and froth gas. Simple hand calculations can be made of the resulting voiding. These are discussed in Section A.3. In addition, we used the UVAFCI[3] code for similar calculations (Section A.4) which brought in the effect of frictional losses and backpressures in restricting voiding. In cooperation with L. Lois and J. Meyer of DPM we then selected appropriate input parameters to model the voiding using SAS3A. (See Section A.5.)

A.3 Simple Hand Calculation of LOF-D-TOP Voiding Rates due to Fuel Gasses

Simple calculations such as those presented here can be used to conservatively scope the maximum voiding rates you could expect for cavity-and-froth-gas expansion following a long-rip failure during the LOF-D-TOP.

The calculations make several simplifying assumptions:

1. the inertial constraint consists of two equal-length incompressible slugs,
2. slug motion is frictionless and with negligible backpressure from the inlet and outlet plenum regions,
3. the fission gas expands isentropically, and
4. to simplify the equations, an "average" gas pressure is used over a given total expansion time.

Originally we looked at the acoustic part of the expansion; however, this appears unnecessary in light of the short times involved in the acoustic expansion relative to the overall expansion times.

The equations used in the hand calculations are as follows:

$$P = L\rho \frac{du}{dt} = \frac{L\rho}{A} \frac{d^2V}{dt^2} \qquad (1)$$

where P = gas pressure

L = length of sodium constraint

ρ = sodium density

u = slug velocity

A = flow area for expansion = twice the normal channel area

V = total gas volume

For an isentropic expansion

$$PV^{\gamma} = \text{constant}, C_1.$$

Note that if you insert this expression for P into Equation (1), the resulting equation is not obviously solvable analytically for V. Therefore, we calculated an "average" P to use for expansion to a given final volume, i.e.,

$$\bar{P} = \frac{\int_1^2 P\,dV}{\int_1^2 dV} = \frac{\int_1^2 \frac{C_1}{V^{\gamma}}\,dV}{\int_1^2 dV} = \frac{C_1\left[\frac{V^{-\gamma+1}}{(1-\gamma)}\right]_1^2}{V_2 - V_1}$$

This $\bar{P}$ is then used in Equation (1) to calculate V(t).

$$\bar{P} = \frac{L\rho}{A}\frac{d^2V}{dt^2}$$

$$\bar{P}t = \frac{L\rho}{A}\frac{dV}{dt} + C_2$$

If we assume the slug velocities are zero at t = 0, we have

$$\frac{dV}{dt} = 0 = C_2, \text{ so}$$

$$\bar{P}t = \frac{L\rho}{A}\frac{dV}{dt} \qquad (2)$$

Integrating again,

$$\frac{\bar{P}t^2}{2} = \frac{L\rho}{A}V + C_3$$

we get C_3 from the value of V at time zero, i.e., $V(0) = V_1$. Then

$$C_3 = \frac{L\rho}{A}V_1, \text{ so}$$

$$\frac{\bar{P}t^2}{2} = \frac{L\rho}{A}(V - V_1).$$

Then match the V in the above equation with the V_2 in the expression for $\bar{P}$:

$$\frac{\bar{P}t^2}{2} = \frac{C_1(V_2^{1-\gamma} - V_1^{1-\gamma})t^2}{(V_2 - V_1)(1 - \gamma)2} = \frac{L\rho}{A}(V_2 - V_1) \qquad (3)$$

Note that equation (3) can be used to determine a voiding history in a backward manner, i.e. insert a value for V_2 and solve for t:

$$t = \left\{ \frac{2L\rho}{A} \frac{(V_2 - V_1)^2(1 - \gamma)}{P_1 V_1^{\gamma}(V_2^{1-\gamma} - V_1^{1-\gamma})} \right\}^{0.5} \qquad (4)$$

Note also from equation (2) that the voiding rates (and therefore the associated reactivity ramp rates) are proportional to t/L, while equation (4) above says that t is proportional to $\sqrt{L}$. Therefore, as a general result, the voiding rates will be <u>inversely proportional to $\sqrt{L}$</u>.

For the calculations discussed below, we used pin failure conditions from a SAS run obtained from DPM personnel. Initial slug velocities were assumed zero consistent with the above development. Selecting an effective slug length, L, which is a very critical parameter as indicated in the preceeding paragraph, was difficult because of the characteristic prefailure boiling in the SAS channels of interest (channels 7 and 8). A choice of slug lengths at various times following failure based on SAS results could range from essentially zero to about 200 cm. For the current calculations we utilized two slug lengths: 50 cm and 150 cm. However, the convenient scaling of voiding rates as $1/\sqrt{L}$ for short times (e.g. a few tens of milliseconds) following pin failure, allows easy extrapolation to other values of L. It is the potentially small effective value of L for the first few milliseconds after pin failure which leads to such large voiding rates in LOF-D-TOP channels, whether the driving force is an FCI or a squeeze-out by fuel gas pressurization.

The first accompanying figure shows total slug motion histories for four cases. Each of the two channels was analyzed for the two different slug lengths indicated above. Equation (4) was used for the calculations, with parameter values indicated below:

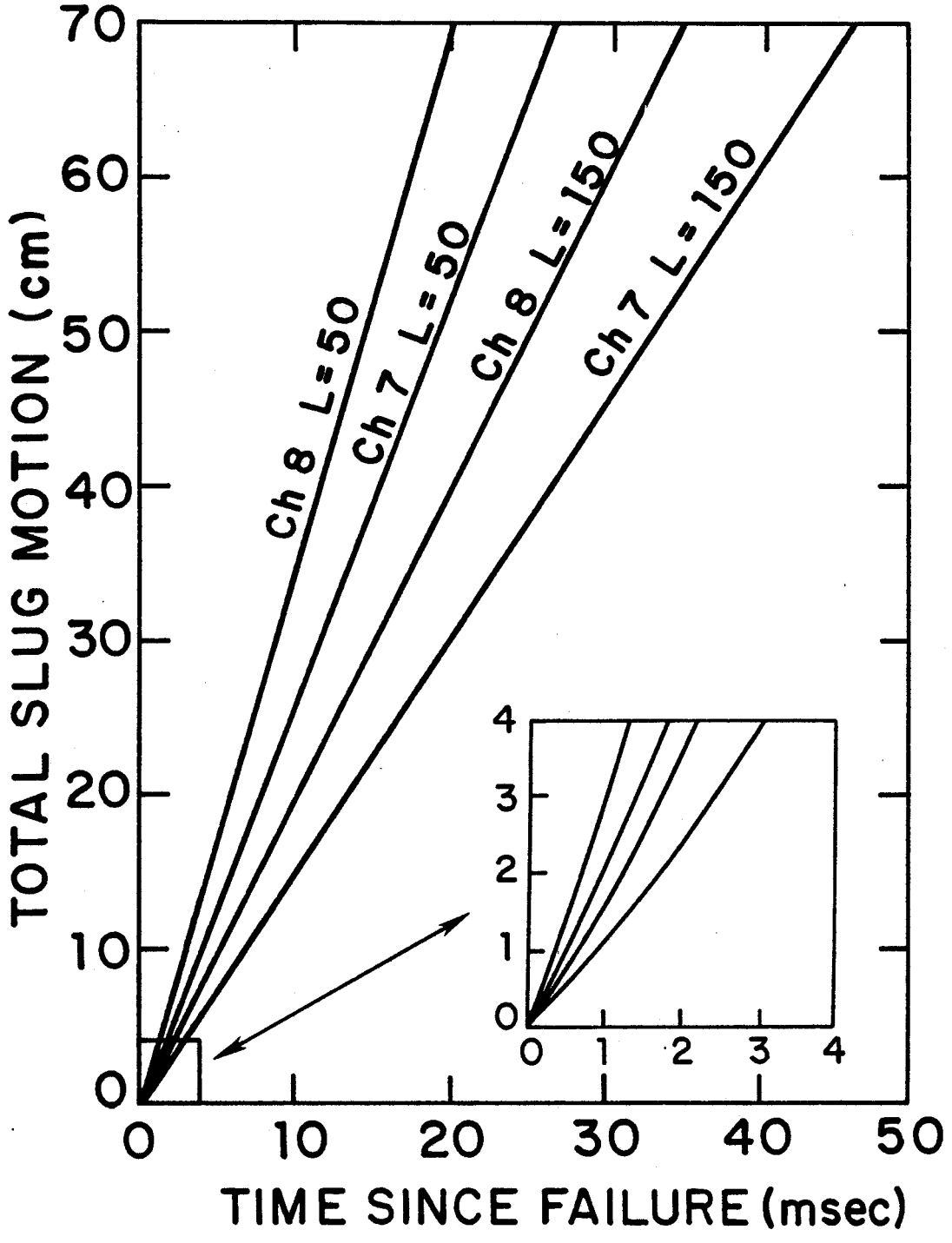

Figure A.1 Motion histories of constraining slugs for two different failure conditions, each analyzed with two different constraining slug lengths.

$A = 0.4\ cm^2$

$\rho = 0.7\ g/cc$

$\gamma = 1.67$

$V_1 = 0.1429$ cc for channel 7
0.0772 cc for channel 8

$P_1V_1^{\gamma} = 9.348\ atm \cdot cc^{1.67}$ for channel 7
$10.694\ atm \cdot cc^{1.67}$ for channel 8

Channel 7 failed first, so the implications of the results for channel 7 presented in Figure A.1 will be discussed in some detail. The rate at which void length is produced during the first 10 msec following failure for the case with L = 50 is about 26 cm/.01 sec = 2600 cm/sec. The void worth per unit length in channel 7 is 1.8 ¢/cm near the center of the pin. This translates to a ramp rate of about 45 $/sec; the total reactivity added in the first 5 milliseconds is about 22¢. Looking at the channel 7 case with L = 150, the corresponding numbers at 5 milliseconds after failure are reduced by approximately $\sqrt{150/50} = \sqrt{3}$, i.e. 26 $/sec and 13¢. Assuming L = 200 cm (excessively long) would still have resulted in 22 $/sec and 11¢ over the first 5 milliseconds, while L = 25 cm would give 64 $/sec and 32¢.

This vigorous voiding in channel 7 in <u>not</u> the result of releasing a large fraction of the intragranular gas from the fuel during the transient. Only 16.1 milligrams of gas were involved, 7.3 milligrams of which were in the original central void. (There should probably be much more than this .0073 g in the central void as discussed in Section A.6, item 1.) A <u>single</u> axial node in SAS near the center of the pin contained the order of 20 milligrams of gas at steady state. Therefore, 16 milligrams is not a massive, unrealistic total release. The question of release rates is addressed in Section A.6, item 3.

The next step in our investigation of the voiding possibilities was to utilize the UVAFCI code in order to better model constraint geometry and look at the effects of frictional forces and opposing back pressures on slug motion. Note that it would be easy to simulate an average backpressure in the simple hand calculations outlined earlier. If the average backpressure is $\bar{P}_b$, equation (4) would be changed to:

$$t = \left\{ \frac{2}{(\bar{P} - \bar{P}_b)} \frac{L\rho}{A} (V_2 - V_1) \right\}^{0.5}$$

$$= \left\{ \frac{2L\rho}{A} \left(\frac{P_1 V_1^{\gamma} (V_2^{1-\gamma} - V_1^{1-\gamma})}{(1 - \gamma)(V_2 - V_1)} - \bar{P}_b \right)^{-1} (V_2 - V_1) \right\}^{0.5}$$

but this would only be useful in the above form for $\bar{P} \geq \bar{P}_b$.

A.4 UVAFCI Calculations of Fuel Gas Voiding

The hand calculations described in Section A.3 use adequate constraint models in characterizing initial voiding rates, but do not consider frictional effects. Moreover, the driving pressure is only approximate because of the use of a volume-history-averaged gas pressure. We decided to check the voiding rates by utilizing the UVAFCI code with fuel-to-sodium heat transfer surpressed. This also enabled us to use channel geometries and conditions (area changes, upper and lower slugs of different lengths, inlet and outlet pressures of different magnitudes, etc.) more prototypic of CRBR.

Four cases were run to parallel the four cases of Section A.3. Figure A.2 compares the results of the channel 7, L = 50 cm case from Figure A.1 with the UVAFCI results for the same SAS channel and an upper slug length of 50 cm. For times less than 10 milliseconds after failure, the hand calculations and UVAFCI give essentially identical results.* Figures A.3 and A.4 provide more detailed information on the UVAFCI run for which the net constraining slug motion is shown in Figure A.2. The interface positions referred to in Figure A.3 are the locations of the bottom of the upper slug and the top of the lower slug which are initially located at the top and bottom of the failure region at the time of pin failure. The void formed would be located predominantly at the failure location and would not be spread uniformly over the distance between

*Within the first 2 to 3 milliseconds after failure, slug motion is slightly greater for the UVAFCI run, but this fine detail is not clear from Figure 2. The greater slug motion does result in slightly higher peak ramp rates for the UVAFCI run as noted in the text.

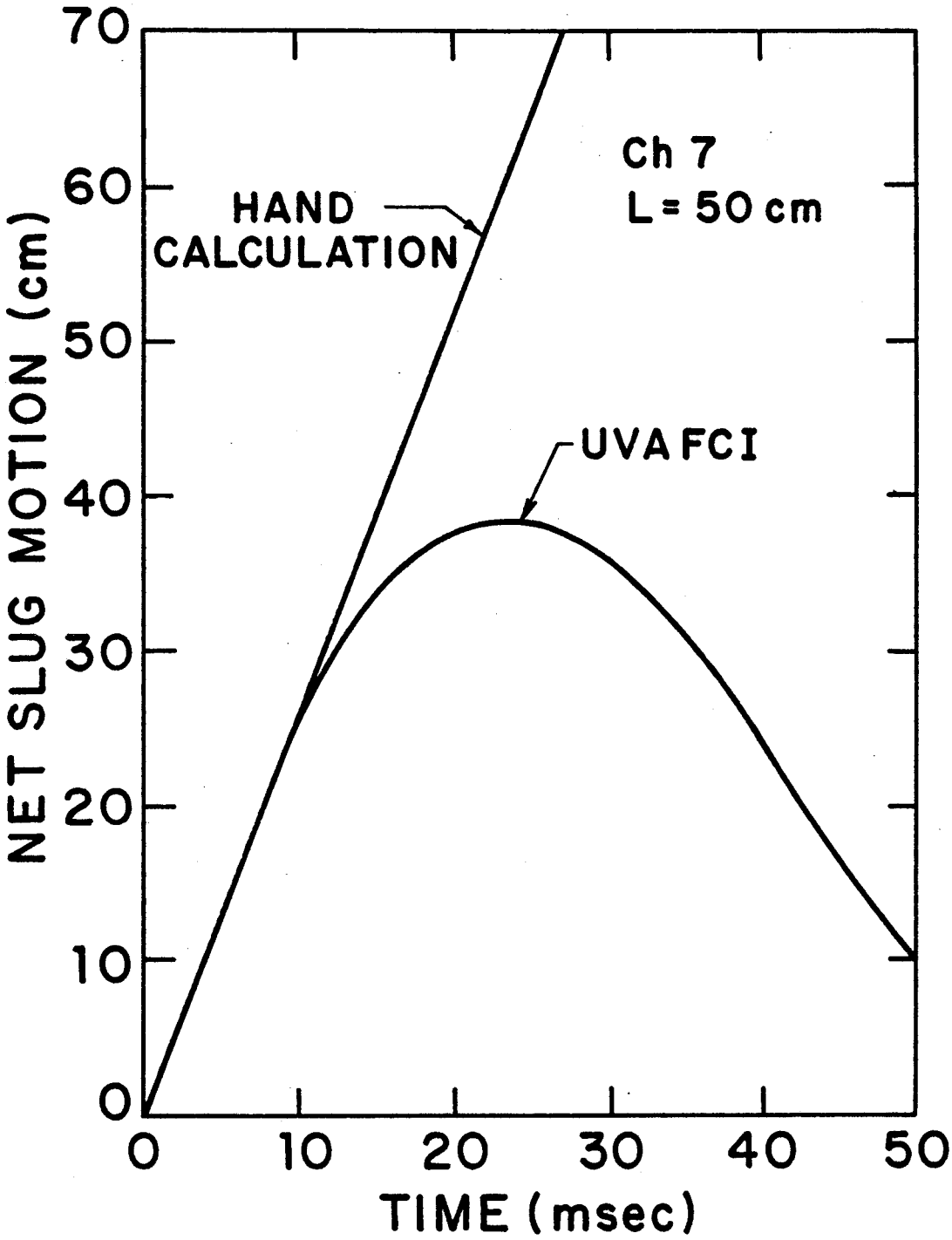

Figure A.2 Comparison of slug motion histories from approximate analytical method and from UVAFCI calculations.

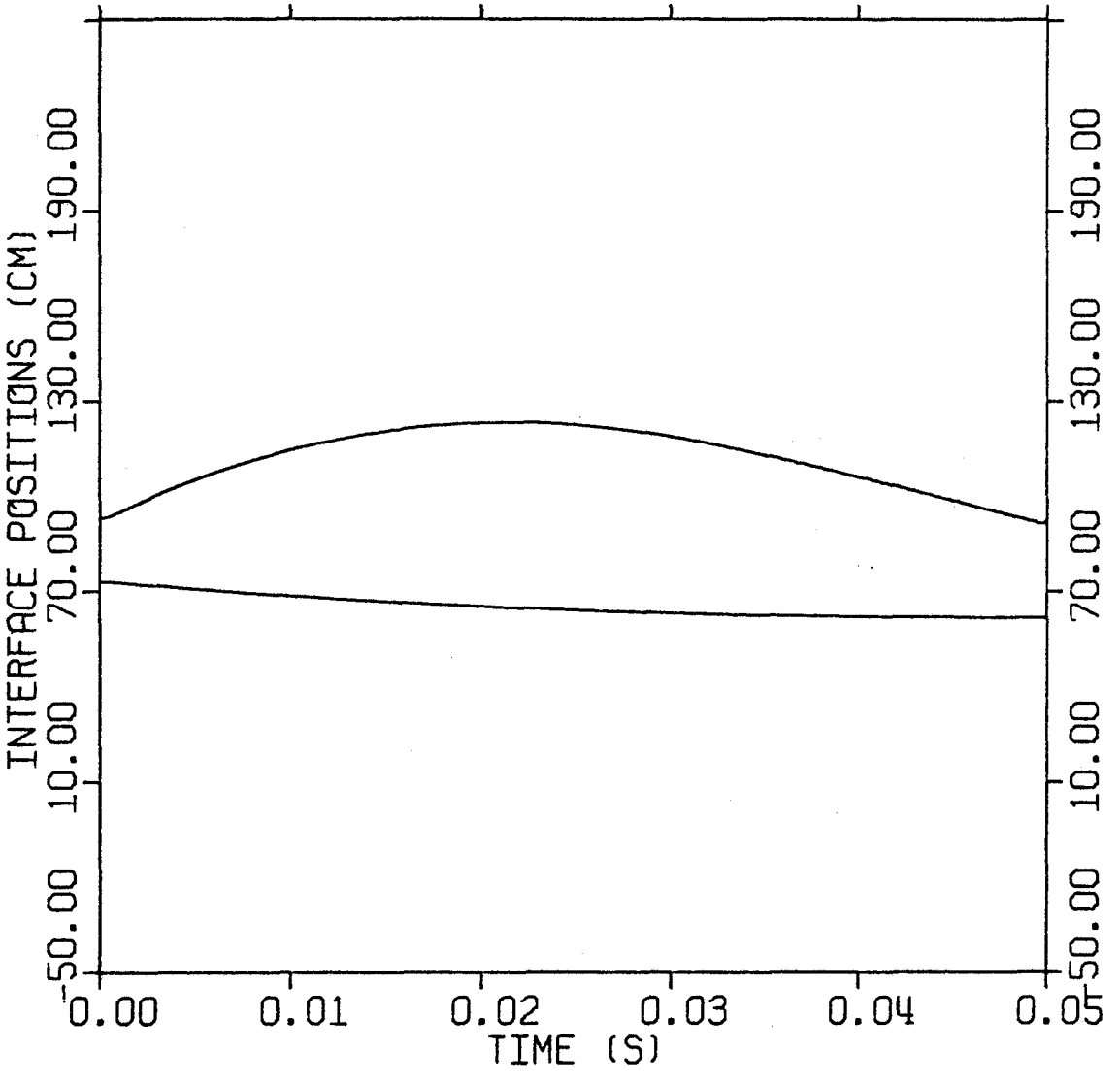

Figure A.3 Interface position histories for channel 7 with a 50 cm upper slug.

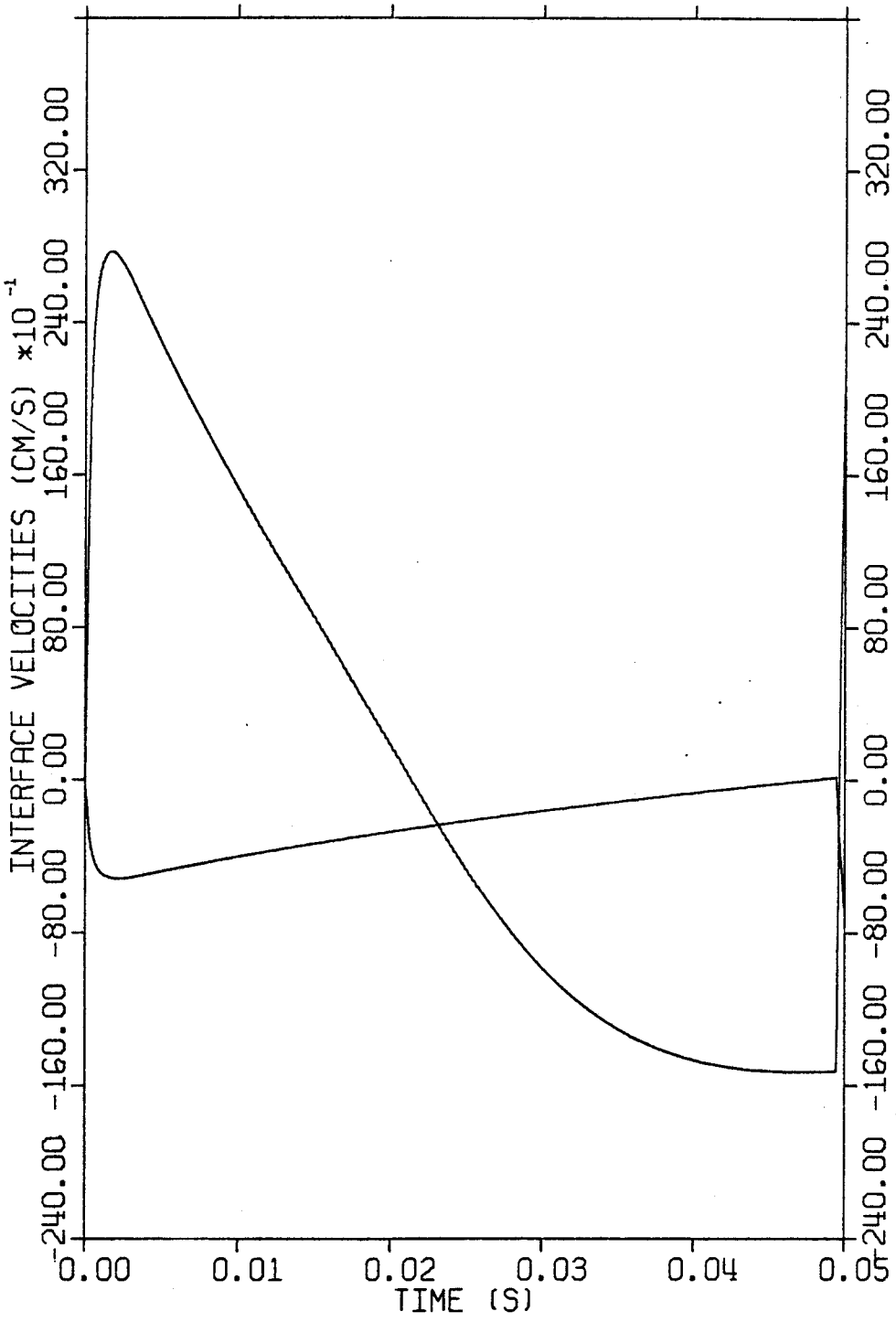

Figure A.4 Interface velocity histories for channel 7 with a 50 cm upper slug.

interface locations. A 20 cm long failure region centered about the axial midplane was considered in all the UVAFCI cases reported here.

We actually feel that the failed region could be much longer than this, perhaps as long as 50 cm; however, in both UVAFCI and SAS/FCI, any sodium considered to be in the rip zone is not included in the inertial constraint. Therefore we selected a failure length which, when used in SAS, would provide a compromise between the desired long rip and reduction in effective constraint.

Figure A.4 can be used to estimate voiding reactivity ramp rates at various times after failure by subtracting the velocities and multiplying by 1.8 ¢/cm. A peak value of 60 $/sec occurs about 2 milliseconds after failure, but after 6 milliseconds the ramp rate has dropped to 45 $/sec with a total addition of 30¢. The ramp rate would actually become negative if the analysis is extended to 23 milliseconds after failure. This is due to the assumption made in the calculation that the backpressures opposing slug motion, both upward and downward, were constant and equal to 4.25 atm. When longer upper slugs are modeled, the ramp rates are lower, but the backpressures are less important. This is illustrated in Figures A.5 and A.6, where the results for channel 7 with a 150 cm long upper slug are shown.

From Figures A.5 and A.6 we see that the peak ramp rates for the 150 cm slug are smaller ($\sim$ 40 $/sec vs. 60 $/sec) and occur later ($\sim$ 3 vs. 2 milliseconds), but the ramp rates continue positive much longer. At 6 milliseconds, $\frac{d\rho}{dt} \sim 30$ $/sec and $\rho \sim 20$ ¢, compared to 45 $/sec and 30¢ for a 50 cm upper slug.

For the channel 8 cases, voiding rates were higher than for channel 7; however, centerline sodium worths are smaller by about a factor of three. The result was peak ramp rates of about 30 $/sec and 20 $/sec for the 50 cm and 150 cm upper slugs, respectively.

It becomes clear from the calculations we have discussed and presented here that the gas voiding can be extremely vigorous and that the length of the upper slug is the controlling factor in initial voiding rates. If LOF-TOP were calculated in channels where the voiding patterns were

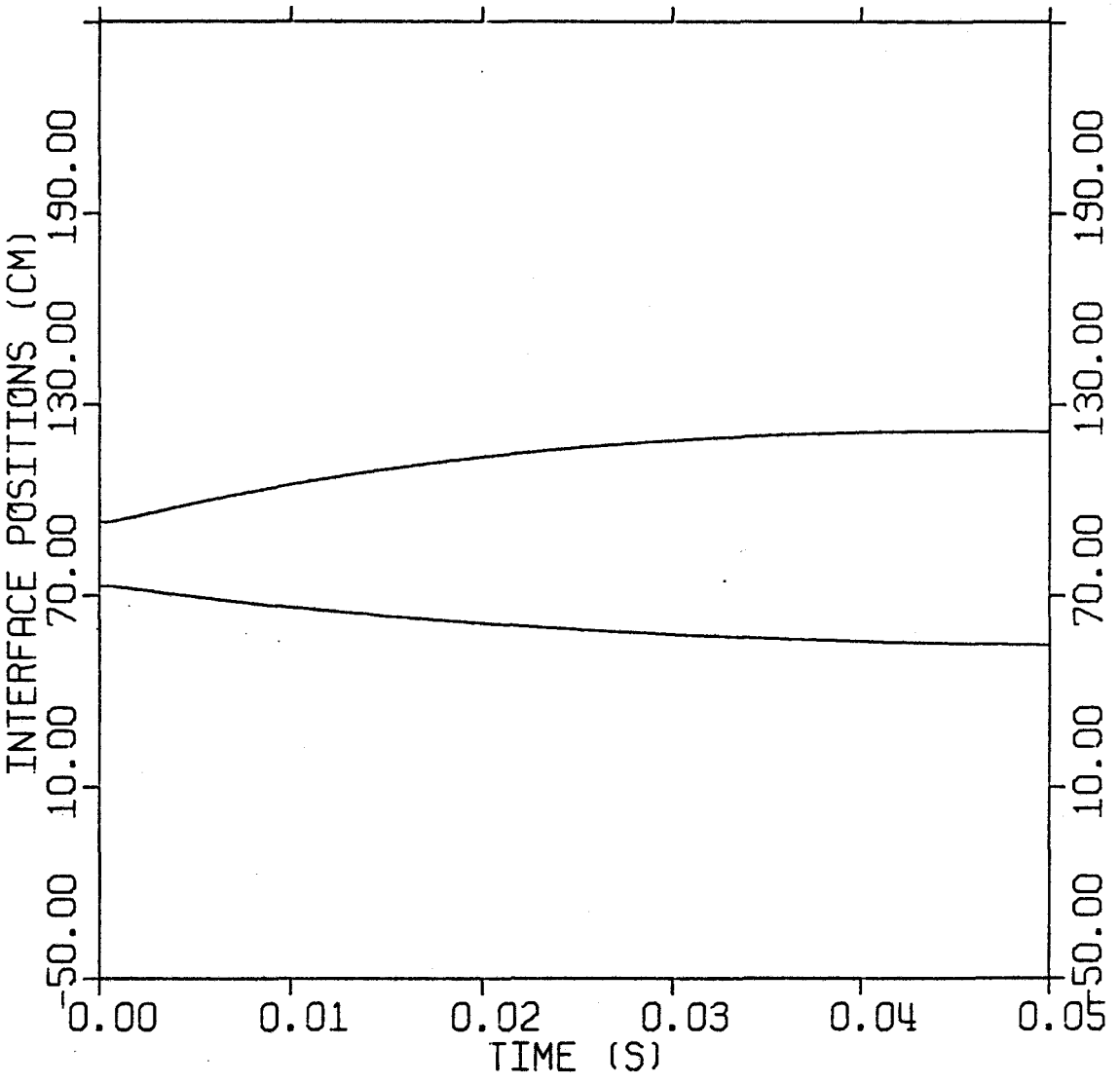

Figure A.5 Interface position histories for channel 7 with a 150 cm upper slug.

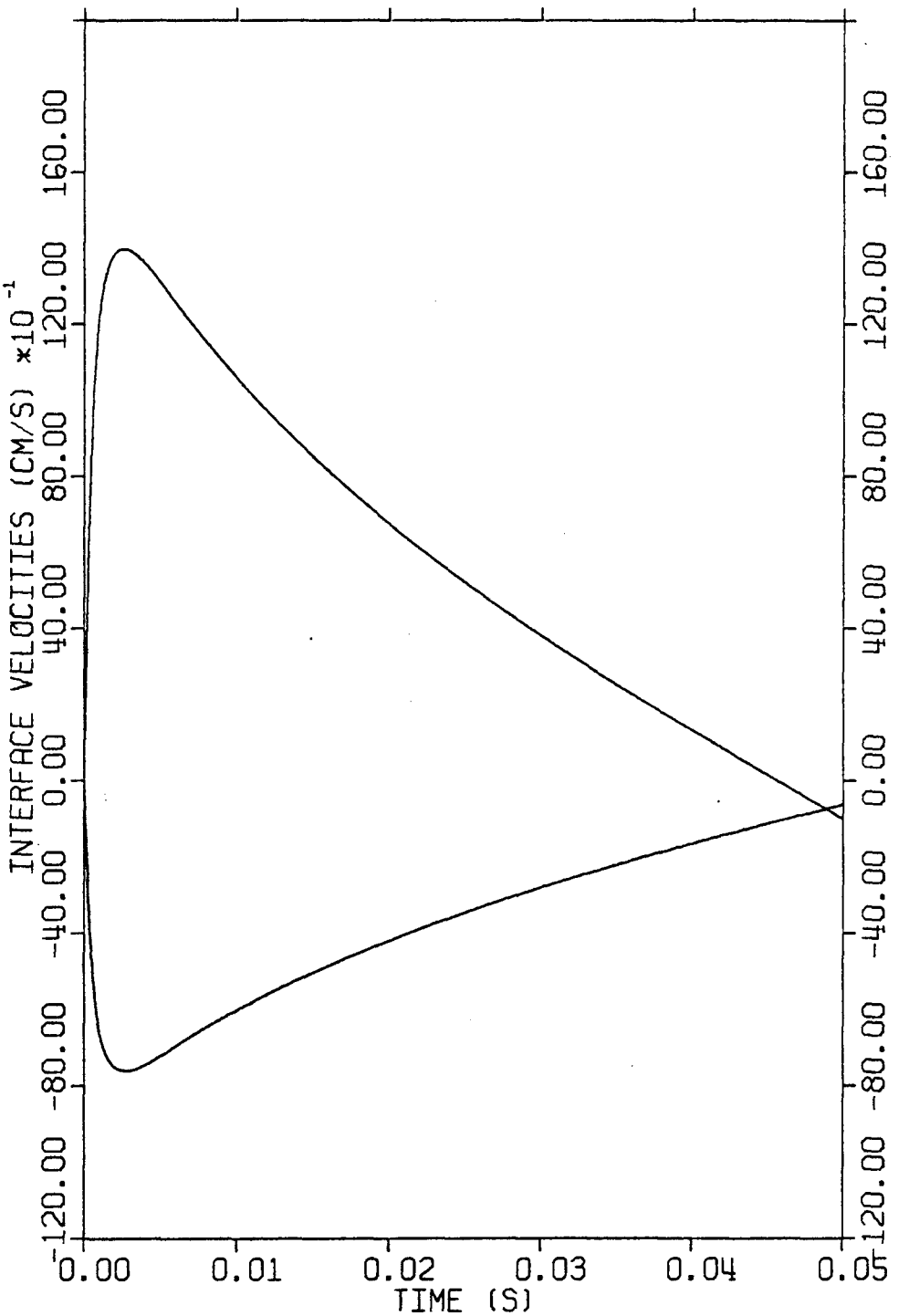

Figure A.6 Interface velocity histories for channel 7 with a 150 cm upper slug.

considerably different at the time of failure than those used here, the resulting voiding histories (and reactivity histories) would also be quite different.

We suggested to DPM personnel that they attempt to model this fuel-gas-induced sodium voiding using SAS/FCI. That effort is discussed briefly in the next section.

A.5 SAS Modeling of Fuel Gas Pressurization

After doing the calculations discussed in Section A.3 and A.4, we felt that there were advantages to performing similar calculations using SAS. First of all, the upper slug length would be handled in a dynamic fashion i.e. if some voids were collapsed with resulting formation of longer slugs during the expulsion process, SAS would account for the change automatically. Also the backpressures which oppose the voiding would be treated in the appropriate time-dependent manner. A third advantage is that the reactivity feedback due to the voiding and the effect of this feedback on the overall accident sequence is calculated in SAS.

Three major input modifications for the SAS/FCI module are needed to model this voiding due to pin "ballooning" or the large scale extrusion of fuel into the channel. First of all, fuel-to- sodium heat transfer must be suppressed (e.g. by using very large particle radii if the conduction model is used). Then, easy, rapid communication must be established between the pin internals and the coolant channel in order to assure essentially no pressure difference between the pin and the channel. This is done by using a large rip area (2 cm^2) and decreasing the inertial length for fuel ejection (1 cm).

With those input changes, DPM personnel were, indeed, able to produce the rapid voiding and associated large reactivity ramp rates we saw in the calculations of Sections A.3 and A.4. Some caveats concerning the general validity of the calculations of these three sections (A.3, A.4, and A.5) will be made in our closing Section A.7. Next we will address some specific questions which ANL personnel raised concerning the calculations.

A.6 Discussions of Specific Uncertainties

In a working meeting with DPM personnel in early July 1976, ANL personnel raised several criticisms concerning analyses of the type presented in the preceeding sections. Some of these are discussed below. Note that items 1, 2 and 3 are closely related.

1. The cracking model was not used in SAS calculations.

If a comprehensive fuel cracking model were used throughout the SAS calculations, i.e. for steady-state as well as transient analysis, the resulting gas voiding would likely be even more vigorous than that calculated above. This is because much of the residual gap volume predicted by SAS at steady-state would really be part of the central void as a result of repeated cracking, fuel creep, and associated gap closure which take place in normal operation. Moreover, for the low power channels important to the LOF-D-TOP, the SSFUEL module of SAS underestimates central void volumes in an additional way: restructuring is calculated based on end-of-cycle pin powers. (The improper gap modeling may actually compensate in part for this last effect.)

In the real fuel pin then, the large amounts of central void gas would have more potential voiding capability (or fuel ejection capability) at failure than the gas in the pins modeled in the previous sections. Thus, we have probably underestimated rather than overestimated gas effects.

2. A 50% melt fraction failure criterion was used rather than the burst pressure failure criterion.

There are several factors which make the use of the 50% melt fraction criterion a reasonable one. First of all, high fuel temperatures and large melt fractions are needed to obtain significant gas release even with Gruber's gas release model.[4] Presumably, then, even the burst failure criterion (with fuel cracking) would require a fairly high melt fraction for failure in a non-voided section of the channel. (Recall that SAS/FCI requires a non-voided channel adjacent to the failure area.)

Perhaps the most important reason not to rely on the burst pressure criterion is that the cladding behavior characteristics which are needed

to apply the burst pressure criterion are not really known for the high ramp rates predicted. At the same time, the boiling model in SAS may be predicting too high a cladding temperature at locations which the burst pressure criterion would select. With these uncertainties in use of the burst pressure criterion (not including for the moment uncertainties in gas release rates which are discussed below), it seems at least as reasonable to specify melt fraction for failure as to use the burst pressure.

3. The gas release timing in SLUMPY and SAS/FCI are fundamentally different.

At first glance the gas release timing in LOF channels seems overly conservative relative to the LOF-D-TOP channels, but this is not really so. On initiation of slumping calculations, SLUMPY effectively smears the fuel/gas froth across available area regardless of gas release timing assumptions. This smearing implies the same general radial fuel motion that we are modeling in the LOF-D-TOP channels, and which was seen in the FI test[5].

It is possible that fission gas may contribute heavily to early fuel dispersal in LOF channels; however, this has not yet been demonstrated by experimental evidence such as that of the FI test, which did not show significant gas driven dispersal. Modeling of FI-type behavior could be achieved with infinite slip of gas past the fuel. It could also be achieved by the assumption that only small amounts of gas are available on initiation of slumping as was done in the DPM runs. Conversely the argument can be made that the gas which can be quickly released in LOF channels (including central void gas) is released before fuel slumping and that this gas can easily escape from the fuel region because of the lack of cladding restraint.

The situation in the LOF-D-TOP channels is quite different. The fuel/gas mixture, including gas which can be released rapidly and gas present in the original central void, are restrained in place by the cladding until the time of cladding failure. Moreover, what we are modeling immediately after failure during the critical sodium voiding

period, is radial fuel motion as indicated above. The amount of gas needed to produce this motion is small. As pointed out near the end of Section A.3, less than 20 milligrams of gas is needed, essentially all of which can be in the initial central void. Again we suggest that for a LOF channel, this gas might well have escaped from the unclad fuel before slumping.

We have not specifically addressed the question of the validity of Gruber's model and its predictions for gas release for the LOF-D-TOP channels, but it is worthwhile to note a couple of points in this respect. First of all, the Gruber model has, as yet, been given relatively limited verification. Secondly, the Gruber model applies only to unrestructured fuel. Realistically there could be several milligrams of gas in the restructured fuel, if only due to gradients necessary at steady state for gas migration to the central void plus the rapidly decreasing temperature gradient near the central void[6]. Moreover, as indicated in the response to 1. above, the central void gas alone is probably capable of producing direct voiding or fuel ejection for FCI voiding.

Thus the availability of the order of 20 milligrams of gas at pin failure seems realistic for the LOF-D-TOP channels, while this availability may be harder to argue for LOF channels at initiation of slumping.

4. We have ignored axial fuel motion in the channels.

This criticism has been directly answered in Section A.2 on Pressurization of Fuel Region.

A.7 Closing Comments and Recommendations

What we have tried to demonstrate here is the possibility for rapid voiding in LOF-D-TOP channels due to fuel gas pressurization even without the occurrence of an FCI. This "squeeze-out" behavior, FCI, and the release of plenum gases are three potential driving forces for sodium voiding. The timing of the operation of any of these forces relative to reactivity events occurring in other SAS channels, is, of course, crucial to the behavior of the reactor during the initial prompt critical burst.

It is difficult to rule out any of these three potential voiding mechanisms, or even to establish their relative timing. However, it does seem likely that one of these mechanisms would become operable during the power spike induced by reactivity events in the other SAS channels. Previous FCI voiding calculations[1] or the fuel gas pressurization calculations discussed here may well be conservative because of the assumed intrasubassembly coherence or other parameter choices; that remains to be demonstrated. The potential for voiding from plenum gas release has not been investigated with regard to timing and time scale of releases in the LOF-D-TOP channels.

We suggest that all three mechanisms receive further attention, particularly the role of the plenum fission gas for high burnup channels.

REFERENCES

1. R. E. Alcouffe, L. Lois, J. F. Meyer, T. P. Speis, and T. G. Theofanous, "Further Considerations on the LOF-Driven-TOP accident for LMFBR's," Trans. Amer. Nucl. Soc., 22, 402 (1975).

2. J. F. Meyer, private communication.

3. C. A. Erdman, M. B. Johnson, A. B. Reynolds, "Post-Failure Phenomena in LMFBR TOP Accidents," Quarterly Progress Report for Jan. 1, 1976-March 31, 1976, NRC Contract #AT(49-24)-0158.

4. E. E. Gruber, ANL-RDP-39, p. 7.15 ff (April 1975).

5. R. G. Palm, R. R. Stewart, S. M. Gehl, A. B. Rothman, and A. DeVolpi, "Loss-of-Flow Test F1 on an FFTF-Type Fuel Element," Trans. Amer. Nucl. Soc., 22, 427 (1975).

6. C. E. Johnson, D. V. Steidl, and C. E. Crouthamel, "Distribution of Gaseous Fission Products in Irradiated Mixed-Oxide Fuels," Proc. of Conf. on Fast Reactor Fuel Element Technology, New Orleans, La., April 13-15, 1971, Amr. Nucl. Soc., Hinsdale, Illinois, pp. 603-613.

APPENDIX B

SELECTION OF VALUES FOR HEAT TRANSFER PARAMETERS

In Section 2, three parameters were introduced which were referred to throughout the report as being controlling parameters for the important heat transfer processes modeled in our parametric studies. For the case of fuel-conduction-limited heat transfer, heat transfer rates from fuel to sodium were argued to be proportional to $(FR^2)^{-1}$, where R is the radius of fuel particles, and F is a factor between 0 and 1. F represents the fraction of the particle radius which is appropriate in characterizing the resistance to heat flow within the fuel particle. The third parameter, designated h, is the FCI zone-to-cladding heat transfer coefficient. A discussion of choices for each of these parameters is given below.

B.1 Fuel Particle Radius, R

As discussed in Section 7.3.3, the experimentally observed particle distributions for fragmentation show a mass-mean particle size for the "fines" of approximately 200 μm.[1] This provides a solid basis for our selection of 200 μm particles as a base value for most of our studies.

The use of a Sauter mean diameter could be justified and would result in more vigorous interactions[2] at short times, as would the use of a complete normal Gaussian distribution in particle size. However, the differences from use of the mass-mean diameter rather than the Sauter mean or the full fuel distribution were not considered significant for this small a diameter.

B.2 Conduction Factor, F

In the conduction-limited model, the effective heat transfer coefficient from fuel to sodium is equal to k/FR, where k is the thermal conductivity of the fuel and F and R are as defined above. If F is taken as 1.0, the resulting heat transfer coefficient is 2.55 $W/cm^2 \cdot K$, or about 4500 $Btu/hr \cdot ft^2 \cdot °F$. Reynolds et al.[3] have shown that use of this coefficient significantly underestimates resulting sodium temperatures in the first 2 to 3 milliseconds following fuel-sodium mixing. Selection

of an F value of 0.5 gives results similar to the exact series solution with an actual surface heat transfer coefficient, h, of 10,000 Btu/hr·ft^2·°F.

We selected a value of 0.20 for F based on two considerations. First, the initial transfer to the sodium would correspond to extremely high effective surface heat transfer coefficients. In Reference 3, a series solution with h = 50,000 Btu/hr·ft^2·°F showed behavior which seemed to give a good compromise between the h = 10,000 Btu/hr·ft^2·°F case and a case with h effectively equal to infinity. When using the conduction-limited model, an F value of about 0.2 was needed to reproduce the early heat transfer rates.

Secondly, a value of 0.2 for F can be argued on the basis that, for a spherical particle of radius R and uniform density, half of the mass of fuel lies within the spherical shell of inner radius 0.794 R and outer radius R. This means that the average distance traveled by a unit of heat in being conducted from the particle as the temperature is uniformly lowered is 0.206 R $\doteq$ 0.2 R. Using an F of 0.2 gives an effective value of h which is undoubtedly too large at long times (i.e. large values of the particle Fourier modulus) but is still low at short contact times. It is also noted in Reference 3 that the use of F = 0.2 still gives lower heat transfer than the old ANL-FCI heat transfer expression[4] with very small mixing times.

If one wishes to look at the effect of larger values of F, we suggest consideration of the parametric studies in Section 5 which talked about cases with particle diameters of 632 μm. These studies could also be interpreted as equivalent to any situation in which the term FR^2 is increased by a factor of ten. For example, we could consider this to be an F of 1.0 and an R of $\sqrt{2}$ · (100 μm) = 141 μm, or an F of 0.5 and an R of 200 μm.

In future studies on other effects, we will probably use an F of 0.5 and an R of 100 μm. This will reduce heat transfer rates at very short times after contact but give higher rates at times larger than about 1.5 msec than for the case with F = 0.2 and R = 100 μm. The difference caused by the increased F value has already been investigated and found to be negligible.

B.3 Zone-to-Cladding Heat Transfer Coefficient, h

This coefficient should model all types of heat transfer occurring between the FCI zone and surrounding cladding (and structure). We have always assumed that no direct heat transfer occurs from fuel to cladding. Only sodium-to-cladding heat transfer is modeled. Also, the early zone-to-cladding heat transfer will probably involve mostly liquid sodium; later in the calculation, the volume fraction of sodium vapor in the FCI zone can approach unity. A third complicating factor is that the zone sodium may, in the later stage of the voiding, become cooler than the surrounding cladding and structure. Thus, the direction of heat transfer may be reversed. This possibility has been considered by others.[5]

Haas[6] has argued that sodium-conduction-limited heat transfer in pin bundle geometry would give upper limit h values less than 8.83 $W/cm^2 \cdot K$ (15,600 $Btu/hr \cdot ft^2 \cdot °F$). This is the same order of magnitude as the nominal forced convection coefficients in CRBR. Haas also referred to steady state sodium vapor condensation coefficients of 5.674 $W/cm^2 \cdot K$ (10,000 $Btu/hr \cdot ft^2 \cdot °F$). An initial condensation coefficient as high as 41 $W/cm^2 \cdot K$ (73,700 $Btu/hr \cdot ft^2 \cdot °F$) for a voided region with conduction through a sodium film could be argued if the effect of any noncondensable gasses present (e.g. fission or fill or manufacturing) is ignored. Similar high numbers could be argued for vaporization of the sodium film off the heated wall. (Note that noncondensable gasses would have a retarding effect on condensation but not on evaporation.) In Reference 5, an upper limit of 27.6 $W/cm^2 \cdot °C$ was used by Cronenberg for both condensation and evaporation, and he noted that this value seemed too high for the condensation process.

After considering all of the factors noted above plus the limitation of one coefficient representing all of the processes (i.e. liquid-sodium-to-cladding heat transfer, sodium vapor condensation, and sodium evaporation off the cladding), a value of 5.674 $W/cm^2 \cdot K$ (10,000 $Btu/hr \cdot ft^2 \cdot °F$) was selected for use in fresh pin simulations. This value probably underestimates condensation rates at certain periods but also almost certainly underestimates re-evaporation rates.

The presence of fission gas was allowed for in most of the burned pin calculations by a reduction of the heat transfer coefficient by a factor of three to a value of 1.891 $W/cm^2 \cdot K$. The factor of three was obtained from Reference 7 with an equivalent gas film thickness of 6.5×10^{-5} cm. The 6.5×10^{-5} cm corresponds to 1×10^{-4} g of gas spread over 250 cm^2 of area at a pressure of 4.6 atm and a temperature of 1100 K. Certainly this thickness could be argued to be much larger, since the order of 1×10^{-3} g of non-condensable gas per g of molten fuel is likely and the 250 cm^2 surface area requires voiding more than 100 cm of the channel. Thus we could have justified values for h for condensation in the range of 0.4 $W/cm^2 \cdot K$ and lower.

We would like to suggest that in future work it would probably be beneficial to modify coding so that separate condensation and evaporation coefficients would be utilized. This would be especially important for burned fuel analysis in which the almost certain presence of non-condensable gasses could make condensation coefficients an order of magnitude smaller than evaporation coefficients. There modeling changes should also be accompanied by a treatment of axial variation in initial temperatures of condensing surfaces.

REFERENCES
(Appendix B)

1. A. W. Cronenberg and M. A. Grolmes, "Fragmentation Modeling Relative to the Breakup of Molten UO_2 in Sodium," Nuc. Safety, 16, 697 (Nov.-Dec. 1975).

2. D. H. Cho and W. L. Chen, ANL-RDP-1, p. 8.33 (Jan. 1972).

3. A. B. Reynolds, et al., Second Quarterly Report for the Period March 15, 1972 - June 14, 1972, AEC Contract No. AT(40-1)-4313, University of Virginia, pp. 26-33.

4. D. H. Cho, R. O. Ivins, and R. W. Wright, "Pressure Generation by Molten-Fuel-Coolant Interaction under LMFBR Accident Conditions," Proc. of Conf. on New Developments in Reactor Mathematics, Idaho Falls, CONF-710302, pp. 25-49 (March 1971).

5. A. W. Cronenberg, "A Thermodynamic Model for Molten UO_2-Na Interaction, Pertaining to Fast-Reactor Fuel-Failure Accidents," ANL-7947 (June 1972).

6. P. M. Haas, "Improved Modeling of the Fuel-Coolant Interaction in the Hypothetical Core-Disruptive Accident for the Liquid Metal Fast Breeder Reactor," Ph.D. Dissertation, Nuclear Engineering Department, University of Virginia, p. 138 (1974).

7. Progress Report for July 1974, Fast Reactor Safety Division, Department of Applied Science, Brookhaven Nat. Lab., pp. 6-8.

APPENDIX C

CASE PARAMETER TABLES

Case Name	Fuel				Sodium		h (w/cm^2K)	Initial Cladding Temperature (K)	Initial Interface Parameters			Fission Gas Mass in Zone (mg)
	Mass (g)	Initial Temperature (K)	Particle Diameter (microns)	Mixing Time (s)	Mass (g)	Initial Temperature (K)			Location (cm above bottom of lower blanket)		Velocities (cm/s)	
									Upper	Lower		
1B	3.2	3500	250	0.0	1.6	940	5.674	1000	90	80	700	0.0
2B	1.6	3500	250	0.0	1.6	940	5.674	1000	90	80	700	0.0
3B	3.2	3500	250	0.0	3.2	940	5.674	1000	95	75	700	0.0
4B	1.6	3500	250	0.0	0.8	940	5.674	1000	90	80	700	0.0
2E	3.2	3500	500	0.0	1.6	940	5.674	1000	90	80	700	0.0
3E	3.2	3500	250	0.0	1.6	940	2.837	1000	90	80	700	0.0
4E	3.2	3500	250	0.0	1.6	940	5.674	1000	90	80	700	5.5
8F	3.2	3500	250	0.0	1.6	940	5.674	1000	140	130	700	0.0
1G	6.4	3500	250	0.0	1.6	940	5.674	1000	90	80	700	0.0
2G	6.4	3500	250	0.01	1.6	940	5.674	1000	90	80	700	0.0
3G	3.2	3500	250	0.0	0.8	940	5.674	1000	90	80	700	0.0

Table C.1 Input parameters for preliminary studies.

Case Name	Fuel				Sodium		h (W/cm^2-K)	Initial Cladding Temperature (K)	Initial Interface Parameters		
	Mass (g)	Initial Temperature	Particle Diameter (microns)	Mixing Time (s)	Mass (g)	Initial Temperature (K)			Location (cm above bottom of lower blanket		Velocities (cm/s)
									Upper	Lower	
BOL-1	4.8	3500	632	.005	1.6	1000	5.674	1100	90	80	700
BOL-3	4.8	3500	632	.005	1.6	1000	5.674	1100	90	80	700
BOL-8	4.8	3900	632	.005	1.6	1100	5.674	1100	90	80	700
BOL-9	4.8	3900	632	.005	1.6	1100	5.674	1200	90	80	700
BOL-9H	4.8	3900	200	.005	1.6	1100	5.674	1200	90	80	700
BOL-10H	4.8	3900	200	.005	1.6	1100	5.674	1300	90	80	700
BOL-12H	2.4	3900	200	.005	0.8	1100	5.674	1200	90	80	700

Table C.2 Input parameters for fresh fuel (beginning-of-life) runs.

Case Name	Fuel				Sodium		h ($W/cm^2 \cdot K$)	Initial Cladding Temperature (K)	Initial Interface Parameters		
	Mass (g)	Initial Temperature (K)	Particle Diameter (microns)	Mixing Time (s)	Mass (g)	Initial Temperature (K)			Location (cm above bottom of lower blanket)		Velocities (cm.s)
									Upper	Lower	
BURN-5	9.6	3500	632	.01	1.6	1000	1.891	1100	90	80	700
BURN-5H	9.6	3500	200	.01	1.6	1000	1.891	1100	90	80	700
BURN-6	9.6	3500	632	.01	1.6	1000	1.891	1200	90	80	700
BURN-8	4.8	3500	632	.01	0.8	1000	1.891	1200	90	80	700
BURN-9	9.6	3500	200	.01	1.6	1000	5.674	1100	90	80	700

Table C.3 Input parameters for burned fuel runs.

DISTRIBUTION LIST

Copy No.	
1	Dr. James F. Meyer LMFBR Branch Division of Project Management Nuclear Regulatory Commission 7920 Norfolk Avenue Bethesda, Maryland 20014
2	Dr. Theo G. Theofanous P. O. Box 1625 Lafayette, Indiana 47902
3	Dr. William Kastenberg Associate Professor Energy & Kinetics Department University of California at Los Angeles Los Angeles, California 90024
4	Mr. Daniel E. Simpson Manager, Safety Engineering Hanford Engineering Development Laboratory P. O. Box 1970 Richland, Washington 99352
5	Technical Information Center U. S. Nuclear Regulatory Commission P. O. Box 62 Oak Ridge, Tennesses 37830
6	R. Denise, Assistant Director for Special Projects Division of Project Management U. S. Nuclear Regulatory Commission Washington, D. C. 20555
7 - 16	T. Speis, Chief Liquid Metal Fast Breeded Reactors Branch Division of Project Management U. S. Nuclear Regulatory Commission Washington, D. C. 20555
17	A. Sinisgalli, Liquid Metal Fast Breeder Reactors Branch Division of Project Management U. S. Nuclear Regulatory Commission Washington, D. C. 20555

DISTRIBUTION LIST (Cont.)

Copy No.	
18	M. Silberberg, Chief, Experimental Fast Reactor Safety Research Branch Division of Reactor Safety Research U. S. Nuclear Regulatory Commission Washington, D. C. 20555
19	R. Curtis, Analytical Advanced Reactor Safety Research Branch Division of Reactor Safety Research U. S. Nuclear Regulatory Commission Washington, D. C. 20555
20	I. A. Fischer Madison Hall
21 - 22	E. H. Pancake Clark Hall
23 - 26	C. A. Erdman
27 - 28	A. B. Reynolds
29	J. L. Meem
30	RLES Files